NAVAL POSTGRADUATE SCHOOL

MONTEREY, CALIFORNIA

THESIS

SYNTHESIS AND CHARACTERIZATION OF ALUMINUM-NANODIAMOND COMPOSITE POWDERS BY HIGH-ENERGY BALL MILLING

by

Brian D. Sneed

December 2011

Thesis Co-Advisors:　　　　　　　Sebastian Osswald
　　　　　　　　　　　　　　　　　　Luke Brewer

Approved for public release; distribution is unlimited

THIS PAGE INTENTIONALLY LEFT BLANK

REPORT DOCUMENTATION PAGE		*Form Approved OMB No. 0704-0188*
Public reporting burden for this collection of information is estimated to average 1 hour per response, including the time for reviewing instruction, searching existing data sources, gathering and maintaining the data needed, and completing and reviewing the collection of information. Send comments regarding this burden estimate or any other aspect of this collection of information, including suggestions for reducing this burden, to Washington headquarters Services, Directorate for Information Operations and Reports, 1215 Jefferson Davis Highway, Suite 1204, Arlington, VA 22202-4302, and to the Office of Management and Budget, Paperwork Reduction Project (0704-0188) Washington DC 20503.		
1. AGENCY USE ONLY *(Leave blank)*	**2. REPORT DATE** December 2011	**3. REPORT TYPE AND DATES COVERED** Master's Thesis
4. TITLE AND SUBTITLE Synthesis and Characterization of Aluminum-Nanodiamond Composite by High Energy Ball Milling		**5. FUNDING NUMBERS**
6. AUTHOR(S) Brian D. Sneed		
7. PERFORMING ORGANIZATION NAME(S) AND ADDRESS(ES) Naval Postgraduate School Monterey, CA 93943-5000		**8. PERFORMING ORGANIZATION REPORT NUMBER**
9. SPONSORING /MONITORING AGENCY NAME(S) AND ADDRESS(ES) N/A		**10. SPONSORING/MONITORING AGENCY REPORT NUMBER**
11. SUPPLEMENTARY NOTES The views expressed in this thesis are those of the author and do not reflect the official policy or position of the Department of Defense or the U.S. Government. IRB Protocol number ___N/A____.		
12a. DISTRIBUTION / AVAILABILITY STATEMENT Approved for public release; distribution is unlimited		**12b. DISTRIBUTION CODE** A
13. ABSTRACT (maximum 200 words) High-energy ball milling was studied for the ex situ strengthening of aluminum (Al) with nanodiamond (ND). Al-ND metal matrix composite powders with 5 wt% and 10 wt% nanodiamond were synthesized by high-energy ball milling of the blended component powders. Stearic acid was used as a process control agent to minimize agglomeration of the powders upon milling. A uniform distribution of the ND reinforcement was successfully obtained after milling the powders for a period of ten hours with a ball-to-powder ratio of 30:1 in a SPEX 8000M ball mill. Composition and properties of the Al-ND composite was studied using energy dispersive spectrometry (EDS) mapping, scanning electron microscopy (SEM), X-ray diffraction (XRD), optical microscopy, and nanoindentation techniques		
14. SUBJECT TERMS aluminum, ball milling, high-energy, nanocarbon, nanocomposite, nanodiamond, nanoindentation,		**15. NUMBER OF PAGES** 73
		16. PRICE CODE
17. SECURITY CLASSIFICATION OF REPORT Unclassified	**18. SECURITY CLASSIFICATION OF THIS PAGE** Unclassified	**19. SECURITY CLASSIFICATION OF ABSTRACT** Unclassified	**20. LIMITATION OF ABSTRACT** UU

THIS PAGE INTENTIONALLY LEFT BLANK

**SYNTHESIS AND CHARACTERIZATION OF AL-NANODIAMOND
COMPOSITE POWDERS BY HIGH-ENERGY BALL MILLING**

Brian D. Sneed
Lieutenant, United States Navy
B.S., University of Florida, 2001

Submitted in partial fulfillment of the
requirements for the degree of

MASTER OF SCIENCE IN MECHANICAL ENGINEERING

from the

**NAVAL POSTGRADUATE SCHOOL
December 2011**

Author: Brian Sneed

Approved by: Sebastian Osswald
                Thesis Co-Advisor

                Luke Brewer
                Thesis Co-Advisor

                Knox Millsaps
                Chair, Department of Mechanical and Aerospace
                Engineering

THIS PAGE INTENTIONALLY LEFT BLANK

ABSTRACT

High-energy ball milling was studied for the ex situ strengthening of aluminum (Al) with nanodiamond (ND). Al-ND metal matrix composite powders with 5 wt% and 10 wt% nanodiamond were synthesized by high-energy ball milling of the blended component powders. Stearic acid was used as a process control agent to minimize agglomeration of the powders upon milling. A uniform distribution of the ND reinforcement was successfully obtained after milling the powders for a period of ten hours with a ball-to-powder ratio of 30:1 in a SPEX 8000M ball mill. Composition and properties of the Al-ND composite was studied using energy dispersive spectrometry (EDS) mapping, scanning electron microscopy (SEM), X-ray diffraction (XRD), optical microscopy, and nanoindentation techniques.

THIS PAGE INTENTIONALLY LEFT BLANK

TABLE OF CONTENTS

THIS PAGE INTENTIONALLY LEFT BLANK

LIST OF FIGURES

LIST OF TABLES

THIS PAGE INTENTIONALLY LEFT BLANK

LIST OF ACRONYMS AND ABBREVIATIONS

CNT	Carbon Nanotubes
CS	Cold Spray
EFP	Explosively Formed Projectile
FCC	Face Centered Cubic
HP	Hot Pressing
IED	Improvised Explosive Device
MA	Mechanical Alloying
MM	Mechanical Milling
MRAP	Mine Resistant Ambush Protected
ND	Nanodiamond
NPS	Naval Postgraduate School
O-P	Oliver-Pharr
PCA	Process Control Agent
P-V	Pseudo-Voigt
RPM	Revolutions Per Minute
SEM	Scanning Electron Microscopy
TEM	Transmission Electron Microscopy
W-H	Williamson-Hall
XRD	X-ray diffraction

THIS PAGE INTENTIONALLY LEFT BLANK

LIST OF SYMBOLS

Å	Angstrom
Al	Aluminum
Ar	Argon
μ	Micro
eV	Electron Volt
Fe	Iron
kV	kilovolt
keV	Kilo-electron Volt
mA	Milliamp
MeV	Mega-electron Volt

THIS PAGE INTENTIONALLY LEFT BLANK

ACKNOWLEDGMENTS

THIS PAGE INTENTIONALLY LEFT BLANK

I. INTRODUCTION

A. MOTIVATION AND APPLICATION

The United States is currently involved in two separate counterinsurgency operations in which troop mobility is a key factor to our success. As such, there is a strong need for lightweight, maneuverable tactical vehicles that are highly resistant to improvised explosive device (IED) and explosively formed projectile (EFP) attacks. At the present this need is being met through the use of heavily up-armored Humvees and the new breed of Mine Resistant Ambush Protected (MRAP) vehicles. While somewhat maneuverable, the up-armored Humvees grossly exceed their original design weight and when used in an off road environment vehicle reliability is severely compromised. With a flat undercarriage and flat sides, the humvee is also at a distinct disadvantage when attacked with an IED, typically resulting in catastrophic losses when attacked. Conversely, the MRAP vehicles are highly IED and EFP resistant, but due to the massive quantities of steel armor, the smallest MRAP weighs nearly 10 tons, while the largest is over 25 tons. This massive weight is a large problem in rural Afghanistan where many of these vehicles are operated. Most bridges and many roads in Afghanistan simply cannot support the weight of the heavy MRAPs, and have in fact led to numerous vehicle rollovers. A lighter weight MRAP would therefore improve critical performance parameters, particularly maneuverability and fuel economy.

In a time when the fully-burdened cost of a single gallon of fuel to fill the tank of a combat vehicle in Afghanistan is over $400, any improvement in fuel efficiency can potentially save millions of dollars, and lives. An improvement in vehicle maneuverability would enable troops to reach more remote locations, avoid dangerous IED laden roads and improve survivability in ambush situations.

Reducing the weight of the vehicle while maintaining its survivability could be accomplished through the use of a lightweight armor with high strength,

hardness, and toughness. While lower in weight, polymer armors are generally not as tough as metal armors and less suitable for vehicle armoring. At the same time, materials that exhibit superior hardness are often very brittle, rendering them unsuitable as a matrix for armoring applications. In general, armor with the best ballistic properties is the one that is the hardest, yet does not exhibit brittleness; therefore a lightweight, ductile metal matrix with hard, strong reinforcements could possibly be the answer [1].

B.   METAL MATRIX COMPOSITE THEORY

1.   Strengthening Mechanisms

The strengthening of a crystalline material, such as a metal, can be condensed into one primary idea; limiting the movement of dislocations through the crystal lattice [2]. Two common methods of inhibiting dislocation motion is through dispersion strengthening and grain (or crystallite) size reduction.

In dispersion strengthening, hard, insoluble second phases are incorporated into a metal matrix to form a particle-reinforced metal composite [2]. With the discovery of carbon nanotubes (CNTs), the strongest fibers known to mankind, and nanodiamond (ND), the hardest material found in nature, there is an increasing interest in producing carbon nanostructure-reinforced metal composites. Particle-reinforced metal matrix composites typically possess the metallic properties of ductility, toughness and environmental resistance in combination with the ceramic properties of high modulus and high strength [3]. Using the Ashby-Orwan Equation (Equation 1), we can estimate the increase in yield strength from the dispersion strengthening due to the ND addition.

$$\Delta\sigma_y = \left(0.538\frac{GbV_f^{1/2}}{X}\right) * \ln\left(\frac{X}{2b}\right) \qquad (1)$$

Where $\Delta\sigma_y$ is the increase in yield strength, G is the shear modulus of aluminum (Al), b is the Burgers vector of Al, V_f is the volume fraction of ND, and X is the particle diameter of ND. Following the rule of mixtures equations

(Equations 2 and 3), we can estimate the elastic modulus and thermal conductivity of a particle-reinforced metal matrix composite, in this case an Al-ND composite.

$$E_{composite} = V_f * E_{diamond} + (1 - V_f) * E_{aluminum} \qquad (2)$$

$$k_{composite} = V_f * k_{diamond} + (1 - V_f) * k_{aluminum} \qquad (3)$$

Where E is the elastic modulus, k is the thermal conductivity, and V_f is the volume fraction of ND.

Young's Modulus		
V_f	$E_{composite}$ (GPa)	% increase over Al
0.01	81.50	16.43
0.02	93.00	32.86
0.05	127.50	82.14
0.10	185.00	164.29

Table 1.   Estimated value of elastic modulus for given volume fractions of ND

Thermal Conductivity		
V_f	$k_{composite}$ (W/m-K)	% increase over Al
0.01	265.47	4.93
0.02	277.94	9.86
0.05	315.35	24.64
0.10	377.7	49.29

Table 2.   Estimated thermal conductivity for given volume fractions of ND

Yield Strength		
V_f	$\sigma_{yield, composite}$ (GPa)	% increase over Al
0.01	495.49	98.20
0.02	559.23	123.69
0.05	669.56	167.83
0.10	778.49	211.40

Table 3.   Estimated yield strength for given volume fractions of ND

Density		
V$_f$	Density (g/cm^3)	% increase from Al
0.01	2.71	0.30
0.02	2.72	0.61
0.05	2.74	1.52
0.10	2.78	3.04

Table 4.   Density of Al-ND composite for given volume fractions of ND

As shown in Tables 1 through 4, the increases in elastic modulus, yield strength, and thermal conductivity are substantial for a relatively small volume fraction of ND.

In addition to the increase in strength provided by particle reinforcement, metal matrices can also be further strengthened by reducing the crystal size of the matrix. In the 1950s, E. O. Hall and N. J. Petch independently discovered the relationship between the yield point of low carbon steels and grain size.[2] They found that by reducing the grain size of low carbon steel, that the yield strength increased according to Equation 5,

$$\sigma_{ys} = \sigma_o + k_y * D^{-1/2}$$ (5)

where σ_{ys} is the yield stress, σ_o is the frictional stress required to move dislocations in materials with very large grain sizes (which for Al is 15.69 MPa), k_y is the Hall-Petch slope (which for Al is 0.07 MN/m$^{3/2}$), and D is the grain size [2]. B. Q. Han et al found that reducing the grain size of Al-7.5wt% Mg alloy from 500 nm to 50 nm resulted in an increase in strength consistent with the Hall-Petch Equation [4]. High-energy milling of crystalline materials has been proven to reduce grain size by more than 400%, depending on the milling parameters [5], however, the consolidation method must be carefully chosen to prevent significant grain growth.

2. Consolidation Methods of Mechanically Alloyed Powders

While ball-milling can be used to reduce the grain size of metal powders, the powders must be consolidated in order to form macroscale, structural materials. Powder consolidation to the theoretical densities of a nanostructure-reinforced metal composite without significant grain growth is necessary for many material properties such as mechanical behavior [6]. Two methods that have been proven to minimize grain growth while completing full densification of the mechanically powders are Hot Pressing (HP) and Cold Spray (CS).

a. Hot Pressing

As the name implies, Hot Pressing (HP) involves the simultaneous application of heat and pressure. The powder to be hot pressed is placed in a mold or die, heated and pressed, then held at a specific temperature and pressure for a dwell time and then cooled at pressure until there is no threat of oxidation of the material [7]. HP is nearly always performed in either an inert atmosphere or a vacuum to avoid oxidation of the powder. HP in a vacuum has the added advantage of minimizing the chance of trapped air entrapment as well as degassing it during the initial heat-up of the pressing cycle [7].

HP has been shown to achieve nearly full densities with very little grain growth in a number of material types, such as alloys, ceramics and composites [8]. Additionally, L. Kollo *et al* reported that for 10 and 20 vol% nano-silicon carbide-reinforced Al there was no detectable increase in grain size following HP, although at 5 vol% the grain size increased from 100 nm to 130 nm [5]. Unfortunately HP is a very inefficient process for manufacturing large volumes of material, and the graphite molds typically used are very fragile and require replacement on a regular basis, increasing costs. A schematic of a typical HP unit is shown in Figure 1.
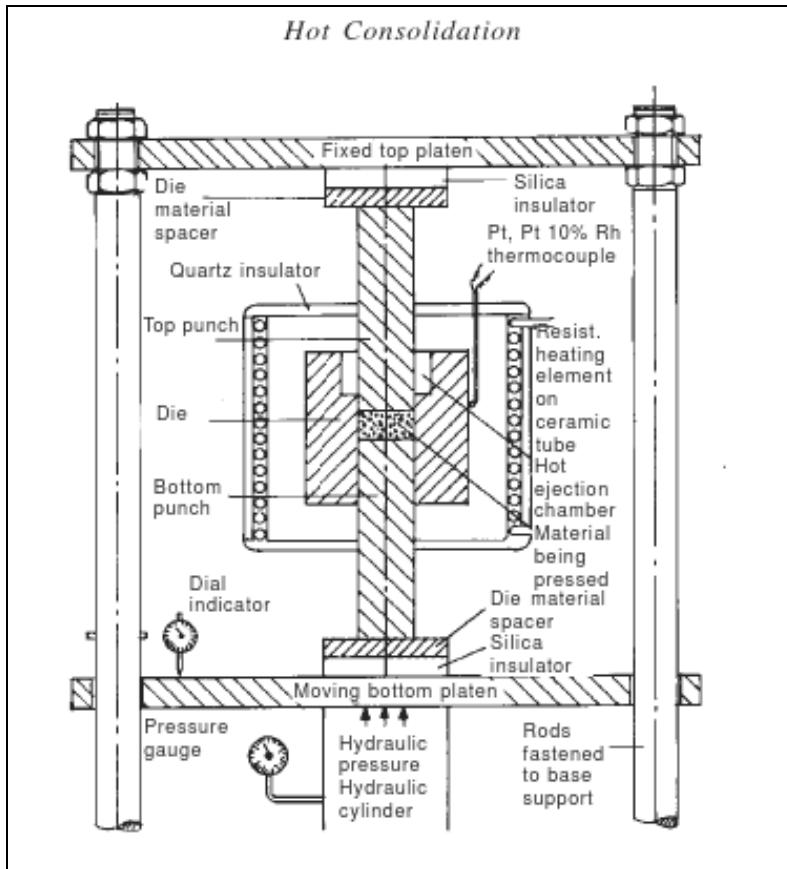
Figure 1.   Schematic of a HP unit [8]

b.   Cold Spray

CS is a powder consolidation method first developed in the mid-1980s by A. Papyrin at the Institute of Theoretical and Applied Mechanics in Novosibirsk, former Soviet Union [9]. Shown in Figure 2 is a diagram of a typical CS System. The high pressure process gas (typically helium or nitrogen) is fed through a gas control module to a manifold system where some of the gas is heated to a preset temperature, while the rest of the gas is fed through a powder-metering apparatus. The purpose of heating part of the gas is not to heat the powder charge (although it may), but to increase sonic flow velocities. The powder-entrained gas stream and the heated gas stream are then fed into a

supersonic nozzle where the combined streams are sprayed onto a substrate to form the coating or deposit [9].
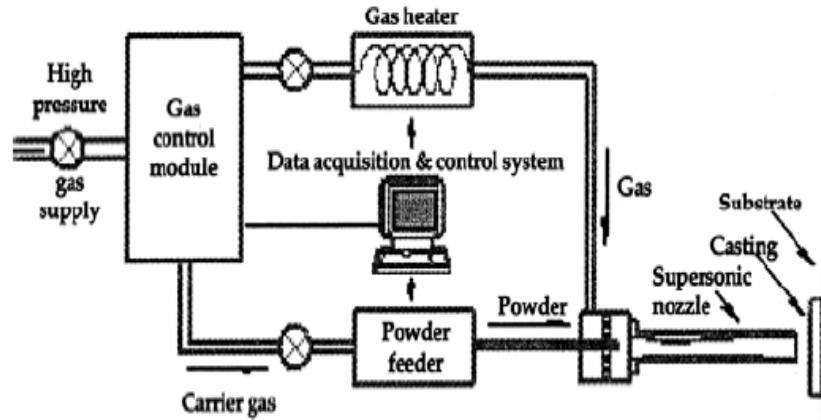
Figure 2.   Diagram of a typical cold spray system [9]

It has been proven that pure metals or composite powders, which include at least one kind of soft composition, are suitable for fabricating high density coatings or deposits through CS [10]. Y. Y. Zhang *et al* reported the successful densification of Al alloy 2009 using a mixture of 30 wt% as-atomized powders and 70 wt% as-cryomilled powders as well as a significant increase in hardening of the cold sprayed coating as compared to the as-cryomilled powder [11].

C.   HISTORY AND BACKGROUND

1.   Mechanical Alloying Overview

Mechanical Alloying (MA) and Mechanical Milling (MM) are two terms commonly used in literature to describe the processing of powder particles in high-energy ball mills. MA is typically used to describe the process of milling two or more different metals or compounds, whereas MM describes the process of milling uniform composition powders such a pure metals [12]. The primary goals of MA include grain size reduction; particle size control; solid-state blending;

7

altering or changing the properties of the material; and mixing or blending two or more materials [3]. Since the late 1960s, high-energy ball milling has been used in industry to successfully manufacture new high strength super-alloys and composite materials.   MA is typically used more often than other fabrication methods, such as rapid solidification, plasma processing, vapor deposition, high pressure torsion and equal channel angular processing, because it can produce the needed materials *in quantity.*   Most of the other techniques are low volume methods used primarily in the laboratory [13].

In milling, energy is imparted to the sample via impacts with the milling media. During the collisions with the milling media the sample is systematically compacted/deformed, cold welded and fractured. It is due to the deformation at high strain rates that causes nanostructured materials to be produced [14]. As milling continues, and the particles decrease in size, the particle fineness approaches a limit. The primary factors leading to the grind limit are: Increasing resistance to fracture, agglomeration, excessive clearance between impacting surfaces, surface roughness of the grinding media, increasing apparent viscosity as particle size decreases, and decreasing internal friction of the slurry as particle size decreases [3].   In the early stages of milling, when mechanically alloying ductile materials (i.e. aluminum) with brittle materials (i.e. nanodiamond), the ductile particles get flattened by the grinding media, while the brittle material is comminuted (though unlikely with ND) [12].   As shown in Figure 3a, these brittle particles tend to become occluded and trapped in the ductile particles and is closely spaced along the interlamellar spacings [12]. As milling continues, the ductile particles get work hardened and the lamellae get convoluted and refined (Figure 3b). With continued milling, if the brittle particles are insoluble in the ductile matrix (such as ND in Al), the lamellae get further refined, the interlamellar spacing decreases, and the brittle particles get uniformly dispersed in the metal matrix (Figure 3c) [12].
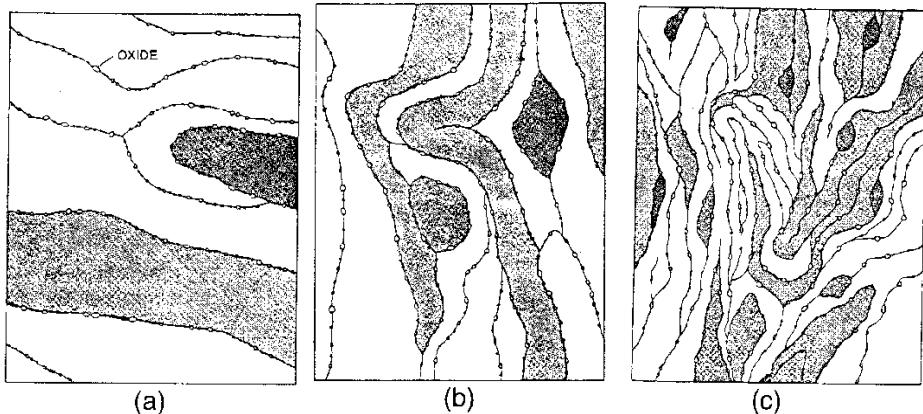
Figure 3.   Microstructural evolution during milling of typical ductile-brittle
combination of powders [12]

2.   Mechanical Alloying Equipment

Milling equipment use for nanoparticle formation and MA can be categorized into four main types of attrition devices; high-energy ball mills such as SPEX type shaker mills, high-energy cryomills, planetary ball mills, and attritor mills. These devices differ in their capacity, efficiency of milling and additional arrangements for cooling, heating, loading, etc. [15]. A brief description and method of mechanical attrition of the different mills is given below.

a.   *High-energy Ball Mills*

The most common type of mill used in the laboratory setting is the high-energy ball mill, such as the SPEX shaker mill. This type of mill uses vials that contain the sample and milling media and shakes them laterally and vertically in such a way that the vial appears to be moving in a figure eight during mill operation. Because of the speed (about 1200 rpm) and amplitude (about 5 cm) of the vibration, the milling media velocities are on the order of 5 m/s, which causes the impact intensity of the media to be very high. For this reason these mills are also known as high energy ball mills [15]. Different sizes of vials can be used to accommodate different sample sizes, with the largest being able to mill

20–30 g of sample. In addition, a number of different vial and milling media materials are available to facilitate milling a wide variety of samples.

b. High-energy Cryomill

Also known as a freezer mill, the cryomill is a cryogenic laboratory mill which chills samples in a bath of liquid nitrogen and pulverizes them with a magnetically driven impactor. Due to the cryogenic temperatures the mill operates in, it can be used for many other uses besides MA, such as medical research, plastics/polymer grinding, DNA/RNA extraction, etc. The mill can grind samples from 0.1 to 5.0 grams. For MA, cryomilling is advantageous because the cryogenic milling temperature limits the effectiveness of recovery in the material, which reduces the time to produce nano-sized grains. It is, however, more difficult and costly to employ due to needing large quantities of liquid nitrogen and near constant monitoring [16, 17].

c. Planetary Ball Mill

Second only to the high-energy ball mill for MA is the planetary ball mill, the most popular being manufactured by Fritsch GmbH in Germany. Like the name suggests, sample containers used in this mill are attached to a support disk and rotate around a central axis, but in addition, the sample container itself also rotates about its own axis, in the opposite direction to the support disk. This combined action causes the centrifugal forces of the vials and support disk to act in alternating like and opposite directions. This causes the grinding media to run down the inside of the vial, causing a friction/grinding effect on the powders, and then when the media reaches inboard location in the spinning vials, the centrifugal forces align and the media is propelled into the opposite wall, causing an impact effect on the powders [12]. This process is most easily visualized in Figure 4. Like the SPEX shaker mills, the planetary milling container and media come in a variety of different materials for grinding or mechanically alloying a number of materials.
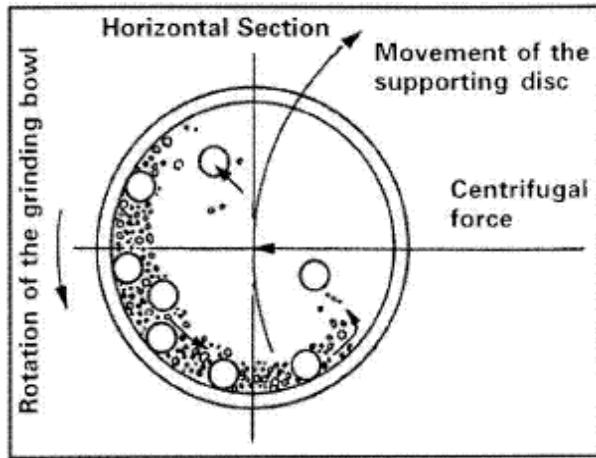
Figure 4.   Ball motion inside a planetary ball mill [3]

d.   *Mechanical Attritor*

A mechanical attritor is a mill that uses a vertical drum with a series of impellers inside it. The spinning impellers agitates the grinding media (balls), causing powder size reduction due to impacts of ball-on-ball, ball-on-container and ball-on-impeller [12]. The attritor impellers spin at approximately 250 rpm, and the typical velocity of the grinding media is approximately 0.5 m/s, therefore the energy imparted to the powders is much lower than in a high-energy ball mill or planetary ball mill [12].

3.   Milling Parameters

Processing parameters such as grinding media type and diameter, ball-to-powder ratio, milling temperature, length of milling, process control agent (PCA) type and use, and proportions of the materials to be mechanically alloyed all affect the final outcome of the milled materials. Additionally, when mechanically alloying materials it is imperative for future research that all milling parameters be clearly documented.

The selection of the type of material the milling media is made of is an important determinant of the efficiency of milling as well as the amount of contamination that will be imparted to the milled material. Contamination is

11

reportedly most serious in highly energetic mills such as the SPEX shaker mills, though the degree of contamination depends largely on the mechanical behavior of the material being milled and its chemical affinity for the milling media [6]. For example, Shen and Koch reported iron (Fe) contamination of nickel, milled for 24hrs in a SPEX shaker mill, at 13.6 wt%, while Niobium, milled at the same parameters developed only 4.03 wt% Fe contamination [10].

The weight of the milling media to the powder, also known as the charge ratio, is a significant variable in the mechanical alloying process. Typical values of the ratio fall in the range of 2:1 to 200:1; however for high-energy ball mills, the ratio is typically in the vicinity of 10:1 [12]. C. Patino-Carachure *et al* milled Al-Cu-Fe powders using an 8:1 ratio [18], whereas S. Filho *et al* used 20:1 and 30:1 ratios for milling Al-Mg powders [19] Varying the ratio significantly will significantly vary the energy imparted to the powder. Filho *et al* reported an increase in particle size when varying the charge ratio from 20:1 to 30:1, and postulated it was most likely due to the higher strain levels. [19]

Milling temperature has been shown to be a significant variable in the constitution of the milled powder. It has been reported that the strain in a material is lower and the grain size is larger for materials that have been milled at higher temperatures [12]. Milling at lower temperatures, such as cryomilling, has been shown to reduce the time required to produce nanocrystalline materials. F. Zhou *et al* reported that milling of Al powder to a grain size of approximately 25 nm took 20 hours in a high-energy ball mill at room temperature, however it took just 8 hours of milling in a Szegvari cryomill to achieve the same result [16].

The length of time a powder is milled is the most important parameter to be controlled. The milling time required to reach optimum particle size reduction will vary depending on the type of milling machine used, the type of material, the ball-to-powder ratio and the temperature of milling [12].

To complete a MA operation successfully, one must ensure that a balance is achieved between the cold welding and fracturing of the powder particles.

Without dispersing a PCA into the powder matrix prior to milling, cold welding will dominate and the particles will agglomerate. A PCA acts as a lubricant or surfactant, absorbs on the surface of the powder particles, and limits cold welding. A typical PCA used in high-energy ball mills is stearic acid, with a concentration of 1-5 wt% of the total powder charge.

D. THESIS OBJECTIVES

The objective of this study is to fabricate Al-ND composite powders for CS synthesis of novel nanocarbon-reinforced armor materials. Specifically, this thesis intends to:

- Determine if mechanical alloying is a suitable technique to fabricate nanodiamond-aluminum composite powders for Cold Spray (CS).

- Determine how milling parameters, such as milling time, ball-to-weight ratio, and nanodiamond concentration, affect the structure and properties of the composite powders.

ND and Al powders will be mechanically alloyed in a SPEX high-energy ball mill and characterized using X-ray diffraction (XRD), scanning electron microscopy (SEM), optical microscopy, and nanoindentation. The primary focus will be on investigating the effects of processing parameters, such as milling time, ball-to-weight ratio, and nanodiamond concentration, on structure and properties of the composite materials.

THIS PAGE INTENTIONALLY LEFT BLANK

II.   EXPERIMENTAL PROCEDURE

A.   MATERIAL PROCESSING

The Al used in this study was -325 mesh, spray-atomized, spherical powder, listed as 99.7% minimum purity (Valimet, Inc., Stockton, CA.), while the ND used was Adamas Nanotechnologies' "Standard nanodiamond", with >98% purity, cubic phase, 4-5 nm primary particle size and 200 nm average agglomerate size. The PCA used was >95% pure, face centered cubic (FCC) phase stearic acid (Sigma-Aldrich Corp., St. Louis, MO.).

The equipment used to MA the as-received micro-Al and ND powders consisted of a SPEX 8000M Sample Prep Mixer/Mill (Figure 5), a SPEX 65 ml, hardened steel vial and 5 mm, hardened steel grinding balls. All samples were weighed using a Denver Instruments scale and then a Vacuum Atmosphere Control, Inc. glovebox (Figure 6) was used to establish an argon (Ar) atmosphere prior to milling.

Figure 5.   SPEX 8000M Sample Prep Mixer/Mill used to mechanically alloy the aluminum and nanodiamond powders.

Figure 6.   Argon filled glove box that was used to establish an argon atmosphere inside the mixing vial prior to milling. An inert, argon atmosphere ensured that there would be no oxidation or oxygen contamination of the mechanically alloyed powders.

To determine if there would be any phase changes to the milled nanodiamond that would reduce its strength, a series of eight milling experiments were completed using just pure ND. From time 0 to 20 minutes, samples were taken at 5-minute intervals, and from 20 to 60 minutes, samples were taken at 10-minute intervals.

From the knowledge gained from a thorough literature review as well running a number of preliminary milling experiments it was decided that a series of 27 milling experiments would be completed in which three milling parameters were systematically varied in an attempt to determine the optimal parameters for producing a composite powder with following ideal properties:

- Average grain size of ~70 nm
- Average particle size of ~50 μm

- Homogenous dispersion of nanodiamond particles

An average grain size of ~70 nm was chosen for two reasons, minimizing processing time and minimizing contamination. D. Oleszak and P. Shingu reported that for Al, the minimum grain size achievable by ball milling is ~25 nm, but required over 100 hours of milling to achieve [20]. During the preliminary experiments for this research, as will be discussed later, it was shown that grain sizes of ~60 nm could be achieved in as little as five hours, which minimizes processing time and potential for powder contamination from the milling media while still providing a large increase in strength from grain size reduction. CS work done by L. Ajdelsztajn *et al* on cryomilled Al 5083 powder showed that an average particle size of 58 μm was sufficiently small enough to be propelled in excess of 700 m/s, which is the critical velocity above which CS deposition takes place [21].

For all experiments, 3.0 %wt stearic acid was added to the powder mixture as a PCA to prevent agglomeration. Table 5 shows the experimental matrix used for systematically varying the ball-to-powder ratio, the milling time, and the weight percentage of ND incorporated.

Experiment	ND Concentration	Ball/weight Ratio	Milling Time
AlNd-1-1	0%	10:1	1hr
AlNd-1-2	0%	10:1	4hr
AlNd-1-3	0%	10:1	10hr
AlNd-1-4	0%	20:1	1hr
AlNd-1-5	0%	20:1	4hr
AlNd-1-6	0%	20:1	10hr
AlNd-1-7	0%	30:1	1hr
AlNd-1-8	0%	30:1	4hr
AlNd-1-9	0%	30:1	10hr
AlNd-2-1	5%	10:1	1hr
AlNd-2-2	5%	10:1	4hr
AlNd-2-3	5%	10:1	10hr
AlNd-2-4	5%	20:1	1hr
AlNd-2-5	5%	20:1	4hr
AlNd-2-6	5%	20:1	10hr
AlNd-2-7	5%	30:1	1hr
AlNd-2-8	5%	30:1	4hr
AlNd-2-9	5%	30:1	10hr
AlNd-3-1	10%	10:1	1hr
AlNd-3-2	10%	10:1	4hr
AlNd-3-3	10%	10:1	10hr
AlNd-3-4	10%	20:1	1hr
AlNd-3-5	10%	20:1	4hr
AlNd-3-6	10%	20:1	10hr
AlNd-3-7	10%	30:1	1hr
AlNd-3-8	10%	30:1	4hr
AlNd-3-9	10%	30:1	10hr

Table 5. Experimental matrix for determination of optimal milling parameters.

Upon completion of milling, each sample was carefully transferred from the milling container into a labeled sample container for storage until characterization procedures were completed.

B. CHARACTERIZATION METHODS

1. X-ray Diffraction

Approximately 95% of all solid materials are crystalline. When X-rays interact with a crystalline phase of a material, a diffraction pattern is produced. An X-ray diffractometer creates these X-rays (with energies on the order of 200 eV to 1 MeV) and measures the diffraction patterns coming off a sample. The X-rays are created in the X-ray tube, which contains anode and cathode electrodes inside a vacuum chamber. The cathode is a tungsten filament that when heated, emits electrons that are then accelerated toward the anode, which is at ground potential. The Phillips PW1830 Diffractometer used for this thesis uses a copper anode which produces Cu K_α X-ray radiation with an energy of 8.04 keV and a wavelength of 0.1542 nm. When the electrons strike the anode, approximately 99% of the energy is converted to heat, and removed via a chilled water cooling system. The other 1% is converted to X-ray radiation. X-rays are produced when the accelerated electron collides with, and ejects an inner shell electron from one of the anode's copper atoms. When an outer shell electron moves to fill the void, an X-ray photon is emitted [22].

Three primary parts make up a diffractometer, the X-ray source (discussed above), the goniometer, which holds the sample, and the X-ray detector. The constructive interference of the X-rays that are scattered by the crystal planes of the sample form a diffraction pattern that is captured by the detector. The angle between the diffracted beam and the transmitted beam is known as 2θ. The detector moves through a range of 2θ, typically $0° < 2\theta < 170°$, while collecting the diffraction pattern.

XRD analysis was conducted for a more accurate and statistically significant estimate of changes in the average grain size and microstrain of the MA composite powders. For the XRD analysis of the MA powders, a thin film of silicone grease was spread onto a glass slide; a thin film of the composite powder was subsequently deposited on top of the grease. The grease was used

to ensure that powder was secured to the slide during measurements. For all analyses, the diffractometer was operated at a voltage of 35 kV and a current of 30 mA. After each set of data was recorded, the XRD analysis program HighScore was employed to perform a Pseudo-Voigt (P-V) curve fit to each diffraction peak and calculate the full width half maximum (FWHM) value for each peak. Using the Williamson-Hall (W-H) analysis explained below and a Microsoft Excel program the author created, the grain size and microstrain of each as-received and milled sample was calculated.

Any divergence from ideal crystallinity, such as finite grain size and strain leads to broadening of the diffraction peaks. Figure 7 shows the typical peak broadening that occurs following a reduction in grain size.
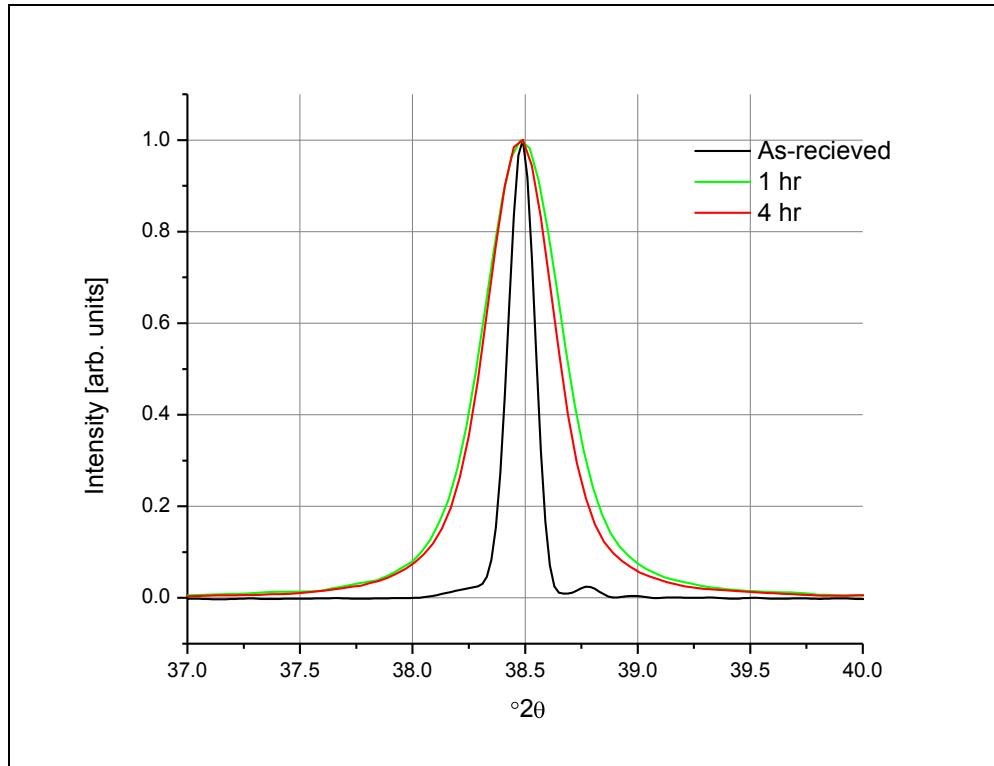

Figure 7.   Illustration of typical peak broadening that occurs due to grain size reduction following milling.

Williamson and Hall developed a method for calculating grain size and strain from diffraction peak integral breadths by using a combination of the

20

Scherrer equation and the Wilson-Stokes equation. Diffraction peak broadening is due to three primary factors—grain size, microstrain, and instrument broadening. To accurately measure grain size and microstrain, the broadening due to the instrument must be removed. This is accomplished by measuring a sample that is well crystallized so that any broadening due to finite size of the grains and microstrain is negligible. With peak broadening due to grain size and microstrain taken out of the equation, the only peak broadening is due to instrument effects and can be subtracted. For the purposes of this research, National Institute of Standards and Technology (NIST) standard sample 660b (lanthanum hexaboride) was obtained and analyzed with the same machine settings as all other samples used in this research. Once analyzed the FWHM of each of the diffraction peaks was plotted and a sixth order polynomial was calculated for the curve, as shown in Figure 8.

$$y = 6E\text{-}11x^5 - 2E\text{-}08x^4 + 3E\text{-}06x^3 - 0.0002x^2 + 0.0045x + 0.0697$$
$$R^2 = 0.9754$$
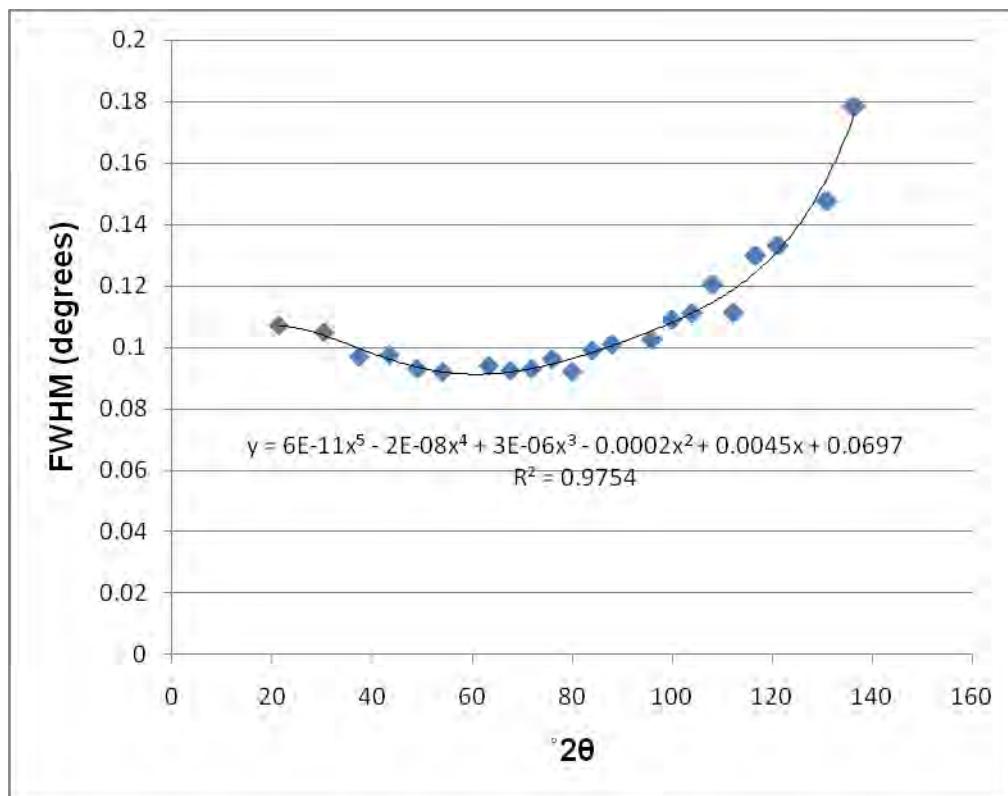
Figure 8.   Plot of FWHM vs °2θ for diffraction pattern of NIST standard sample 660b used to determine instrument broadening.

When measuring diffraction peak widths, most profile fitting programs give FWHM (Γ), but for the most accurate size-strain broadening, the integral breadth (β) should be used. For the P-V profile fitting program used in this research, the integral breadth can be related to the FWHM and is given by:

$$\beta = \frac{(\pi * \Gamma)/2}{\eta + (1-\eta)\sqrt{\pi \ln 2}} \tag{5}$$

where η is a shape factor set at 0.6 by the fitting program [21]. By using the W-H method, one can estimated the grain size (L) as well as the microstrain (ε). As mentioned previously, the observed integral breadth (β_{obs}) is a combination of grain size, microstrain, and instrument effects, therefore to get the true integral breadth (β) the integral breadth due to the instrument (β_{inst}) must be subtracted off.

$$\beta = \beta_{obs} - \beta_{inst} \tag{6}$$

We also know that both grain size (L) and the microstrain (ε) contribute to the integral breadth (β) given by:

$$\beta = \beta_L + \beta_\varepsilon \tag{7}$$

with

$$\beta_L = \frac{K\lambda}{\cos\theta * L} \tag{8}$$

and

$$\beta_\varepsilon = 4\varepsilon \tan\theta \tag{9}$$

Where K is a constant reflecting particle shape (K=1 for spherical particles), θ is the scattering angle and λ is the wavelength of the X-ray radiation (λ = 0.154 nm). Combining Equations 7, 8 and 9, we obtain:

$$\frac{\beta \cos\theta}{\lambda} = \frac{1}{L} + \frac{4\varepsilon \tan\theta}{\lambda} \tag{10}$$

22

To make a W-H plot, one plots $\beta cos\theta/\lambda$ on the y axis and $4sin\theta/\lambda$ on the x-axis. If a linear fit can be achieved, one can extract the grain size from the y-intercept of the fit and the microstrain from the slope. A typical W-H plot is shown in Figure 9.
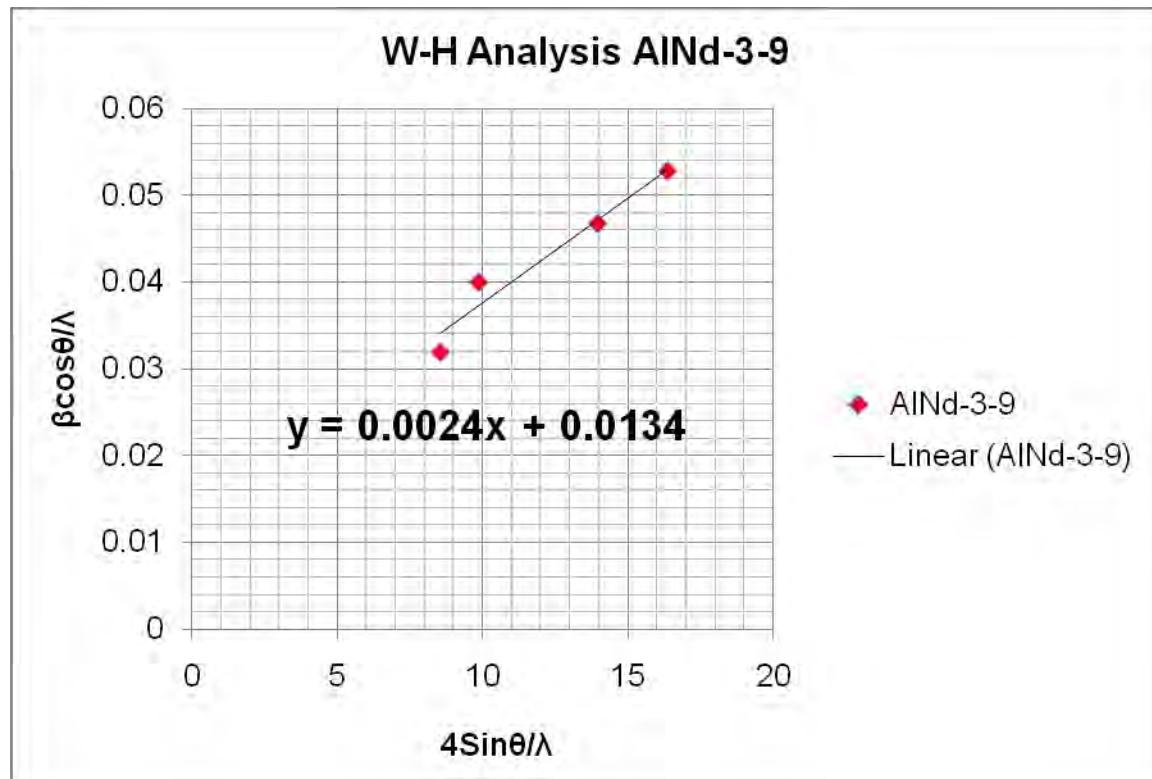
Figure 9.   Typical W-H plot, showing the linear fit of the plotted data, the slope of which is the microstrain and the y-intercept the grain size of the analyzed material.

2.   Scanning Electron Microscopy

SEM is capable of imaging a variety of materials at the nanometer scale by using a focused beam of high-energy electrons that generate several different signals at the surface of the sample. These signals that are created at the electron-sample interaction can be used to characterize the sample's chemical composition, external morphology, and the crystalline structure and orientation of the materials that make up the sample

For characterizing the external morphology of a sample, SEM is a very powerful tool. In contrast to optical microscopy, which has a maximum magnification of approximately 2000X and a minimum resolution of 0.1 μm, whereas SEM has a practical limit of magnification of approximately 75000X and a minimum resolution of 2 nm [23]. The reason for the huge disparity is due to the wavelength of the respective electromagnetic radiation. The minimum resolution of an optical microscope is limited primarily by the wavelength of visible light, which is 390—750 nm, whereas the wavelength of the electron beam used in SEM is approximately 0.5 Å or 0.05 nm. To obtain this resolution the SEM microscope must be operated under a high vacuum to prevent the scattering of the electron beam by gas molecules. To create the electron beam, a cathode filament is heated and electrons are thermionically emitted. The strength of the electron beam is controlled my varying the voltage to the cathode, typically 1 to 40 keV.

When the electron beam strikes the sample surface, scattering events occur. Depending on the type of interaction, the scattering can be either an electron-nucleus interaction (elastic), or an electron-electron interaction (inelastic). The elastic interactions create backscattered electrons (BSE) which give topographical information and, when combined with the characteristic X-rays produced during the inelastic collisions, provide compositional information.

A Zeiss Neon 40 field emission SEM with focused ion beam was used to characterize the topography and chemical composition of select samples. The microscope has a 0.9 nm resolution at 20 kV and is equipped with an Energy Dispersive (EDS) detector and a BSE detector. For SEM analysis, the Al-ND composite samples were mounted on a conductive substrate with carbon tape and then secured to the sample stage of the SEM. For EDS analysis, a small volume of the sample powder was mixed into a small glass vial containing ethyl alcohol. It was thoroughly mixed and maintained in suspension by use of an ultrasonic vibrator. Once mixed a few milliliters of the solution was deposited

onto a copper grid via a dropper and once dry the grid was placed onto the sample stage shown in Figure 10. Prior to being placed into the SEM, all samples were placed in a vacuum chamber for a minimum of 45 minutes to ensure all traces of moisture and air entrapment were removed.
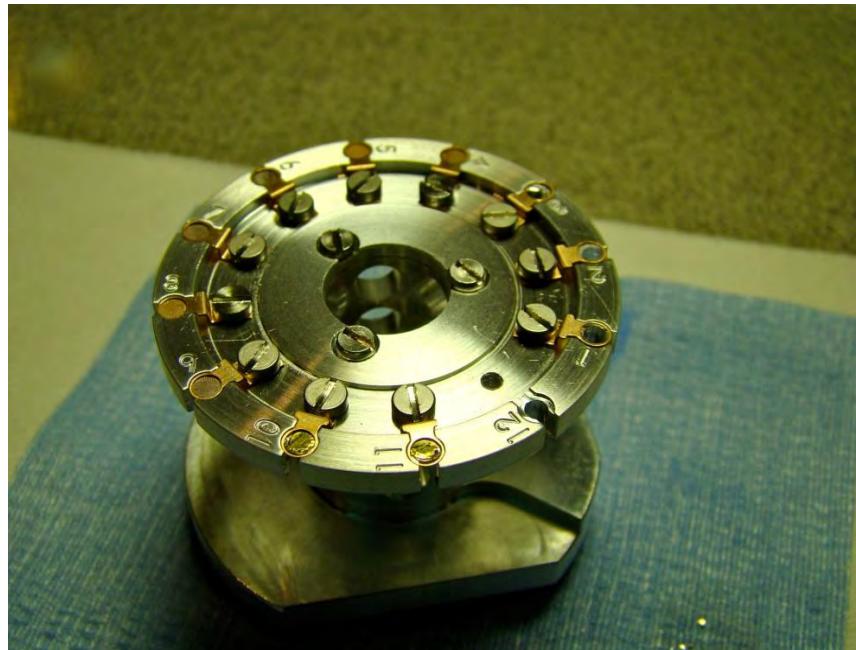

Figure 10.   Sample stage showing copper disks holding minute composite powder samples used for EDS characterization

3.   Nanoindentation

Nanoindentation is an instrumented indentation test that was developed during the mid-1970s as a way to measure the mechanical properties of very small volumes of material. The instrument, known as a nanoindenter, is a very precise, computer-controlled depth-sensing indentation system that allows very small forces and displacements to be measured. The indenter is usually moved via a magnetic coil assembly, and the penetration of the indenter into the sample is measured by an extremely sensitive capacitance gage. As the indenter penetrates the sample, the load, displacement, projected area, and stiffness are recorded continuously. This data is then used to calculate the elastic modulus

and hardness of the sample via the Oliver-Pharr (O-P) method. [24,25]. The O-P method analyzes the elastic modulus according to Equation 11 which originates from elastic theory,

$$E = \frac{\sqrt{\pi}}{2} * \frac{S}{\sqrt{A}}$$ (11)

where E is the elastic modulus, S is the stiffness, and A is the projected area of the elastic contact [25]. The hardness is derived from its normal definition (Equation 12),

$$H = \frac{P_{max}}{A}$$ (12)

where H is the hardness, P_{max} is the peak indentation load, and A is the projected area [25].

An Agilent Technologies Nano Indenter G200 was used for all nanoindentation measurements. The composite powders were prepared for nanoindentation by carefully mixing them into Struers EpoFix, a slow-curing (12-hour) transparent epoxy, particularly suited for vacuum impregnation and mounting very delicate specimens. Once fully cured, the epoxy mounted samples were polished by first using a Buehler HandiMet Roll Grinder, followed by a Buehler standard polisher. Using the high revolutions per minute (rpm) setting of the Buehler Standard Polisher, it was found that the best polish resulted from polishing with the 0.05 µm Al_2O_3 solution for 5 to 10 minutes followed by 10 minutes of the wet felt pad only. Following polishing, the samples were prepared for mounting into the nanoindenter by gluing the samples to the aluminum nanoindenter spacers, as seen in Figure 11.

Figure 11. Photograph showing epoxy mounted, milled composite samples glued to aluminum spacers to allow mounting into the nanoindenter stage.

For all nanoindentation measurements, the *G-Series CSM Standard Hardness, Modulus and Tip Cal* test method of the nanoindenter was used to determine the elastic modulus and hardness of the sample. The indenter uses a Berkovich diamond tip and was calibrated on fused silica. All test settings were set to the default value with the following exceptions: a Poisson's ratio of 0.33, a depth limit of 500 nm, and an allowable thermal drift rate of 0.02 nm/s. Prior to each run, the precise distance between the indenter and the positioning optical microscope was calibrated. Up to twelve individual indentation locations were manually selected from the center of particles on the polished face.

4.   Optical Microscopy

A Nikon Epiphot 200 optical microscope was used to determine milled composite powder average particle size and aspect ratio. Polished samples were imaged at a magnification of 100x power and four images from each of nine samples were recorded. The images were then processed using Image-J software to determine average particle size (cross sectional surface area) and

aspect ratio. For processing with Image-J, the images were first converted to eight-bit format, then made into a binary image, and finally, analyzed with the *Analyze Particles* command which counts and measures the objects in the binary image. To ensure accurate measurements, the program is calibrated by measuring a known distance on the images, which for this case, was the 100 μm scale on a test image.

III.   RESULTS AND DISCUSSION

A.   PRELIMINARY EXPERIMENTS

In order to determine if high-energy ball milling would negatively affect the strength of the ND particulates by inducing a phase change, samples were milled separately for specific time intervals. The diffraction peaks of the as-received ND were found to be exactly the same as that of the ND milled for one hour and ten hours, indicating that no new carbon phases were likely formed during milling. Diffraction peak widths were also measured to determine if there were any changes in grain size of the ND. The diffraction peak widths varied considerably from sample to sample, and no definite trend could be observed, as illustrated in Figure 12, but by comparing the as-received ND against the one hour milled sample as shown in Figure 13, it is clear no verifiable peak broadening is occurring. A three micron micro-diamond sample is shown as well to illustrate the differences in peak widths due to large differences in grain sizes. The <111> ND peak was illustrated because due to the small size of the ND particles and grains, the higher order peaks signals are too weak for such peak width measurements.
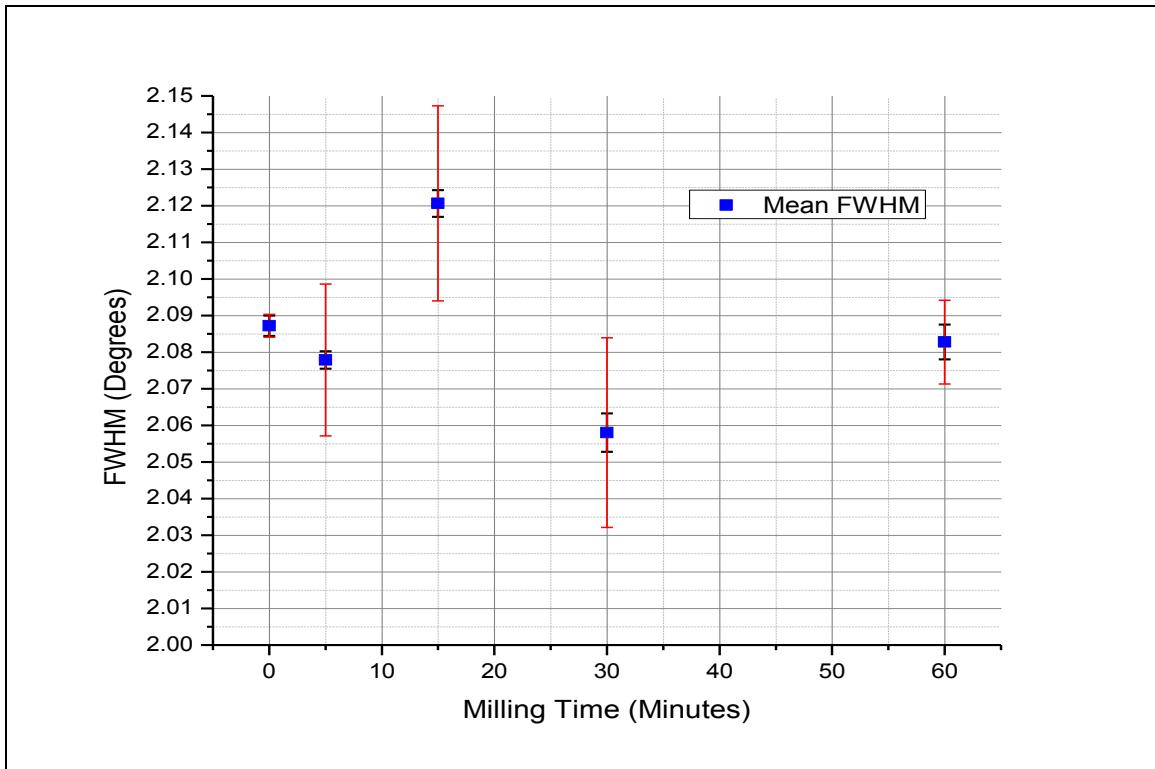
Figure 12.   Mean FWHM values for milled ND powder illustrating the considerable variation in widths.
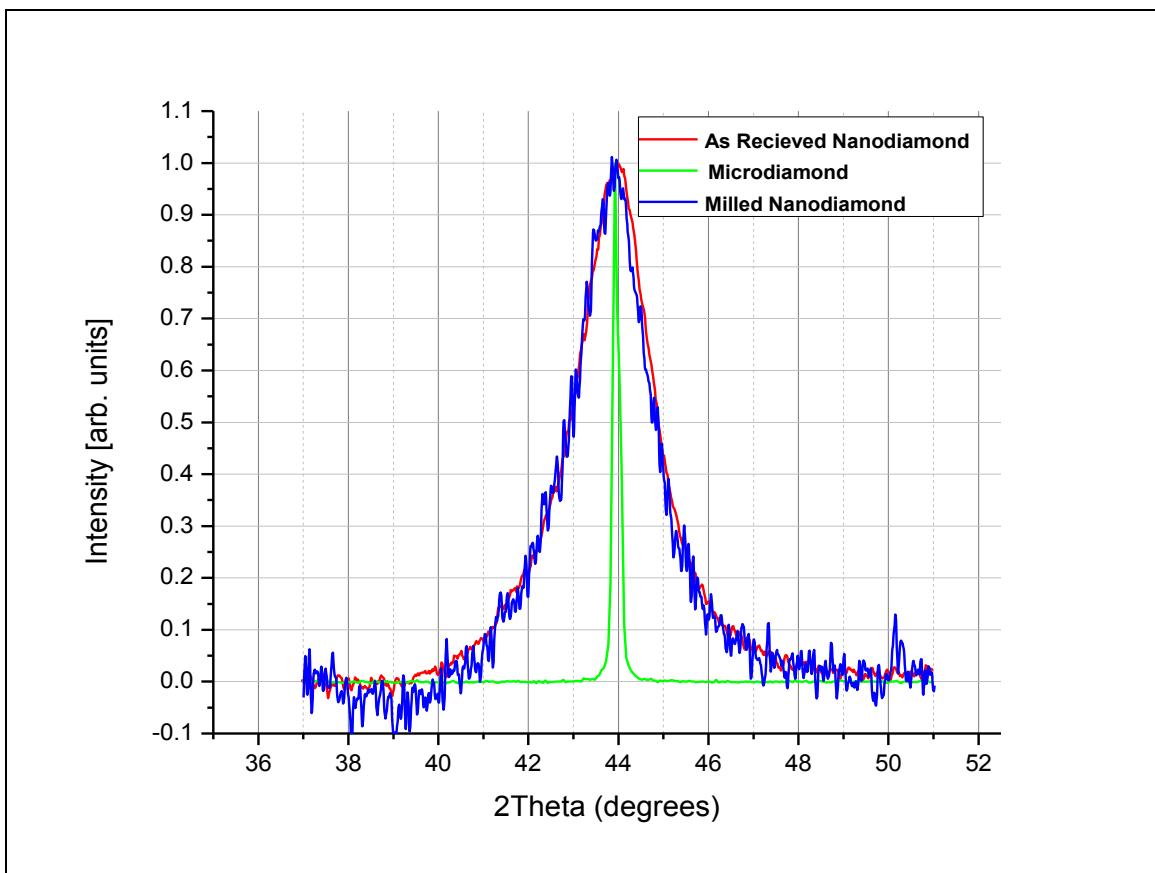
Figure 13.   Plot of the <111> peak of diamond illustrating the negligible peak broadening of one hour milled nanodiamond powder compared to as-received, unmilled nanodiamond and microdiamond.

Although no phase change or grain size changes could be observed with the SEM or XRD machines, it is quite clear there is a visual change in the appearance of the powder, as shown in Figure 14. As milling time increased, the milled powder darkened in appearance. This is likely due to the outer layer of the ND being transformed from SP2 carbon (ie diamond) to SP3 carbon (i.e. graphite), however since only the outermost layer is affected it is so small as to be undetectable by XRD analysis.
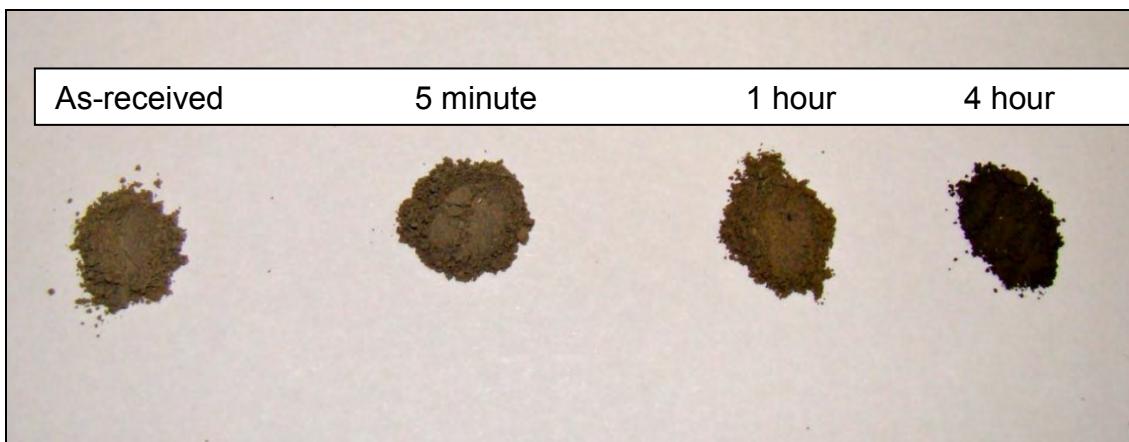
Figure 14.   Photographs showing discernible color change of as-received and milled nanodiamond powder.

Following the ND experiments several milling experiments were performed on the microaluminum powder in an effort to determine the bounds for the primary milling experiments. Samples were milled using a 10:1 ball-to-powder ratio for 1, 2, 3, 5, 10, 15 and 20 hours. Upon completion of milling all samples were analyzed via XRD and a W-H analysis was performed. Based on visual observation of particle size and the W-H analysis for grain size, it was observed that three hours produced the smallest grain size, after which the grain size increased, as shown in Figure 15. With this data it was decided to perform the 27 experiments as detailed in Section II.
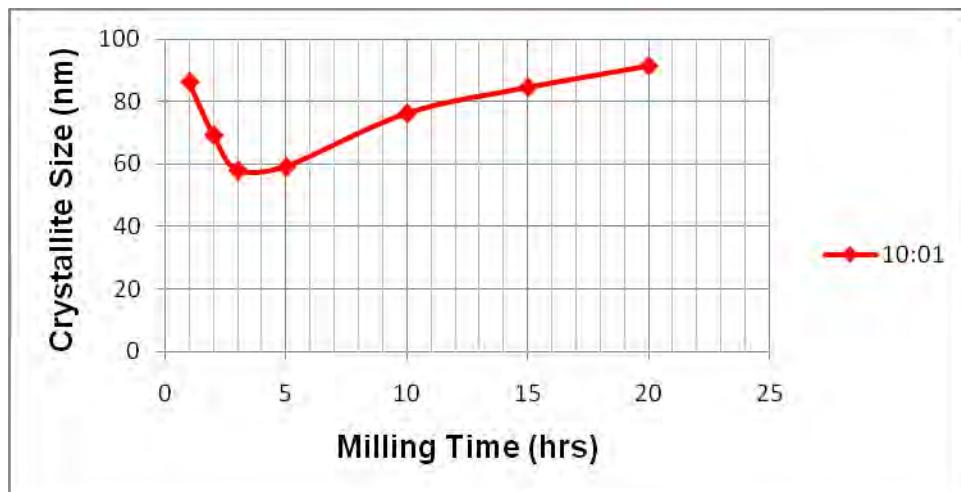
Figure 15.   Plot of average grain size vs. milling time for as received
microaluminum milled at a 10:1 ball to powder ratio.

B.   POWDER MORPHOLOGY AND CHEMICAL COMPOSITION

1.   As-Received Nanodiamond and Aluminum Powders

Presented in Figure 16 is an SEM micrograph of the as-received ND powder. After incorporation into the milling process, these agglomerates broke down quite easily. SEM micrograph of the as-received microaluminum powder is shown in Figure 17. The microaluminum was spherical in shape and had an average particle size of 15 µm.   Both the as-received nanodiamond and microaluminum morphologies and particle sizes agreed with the published manufacturer's data.
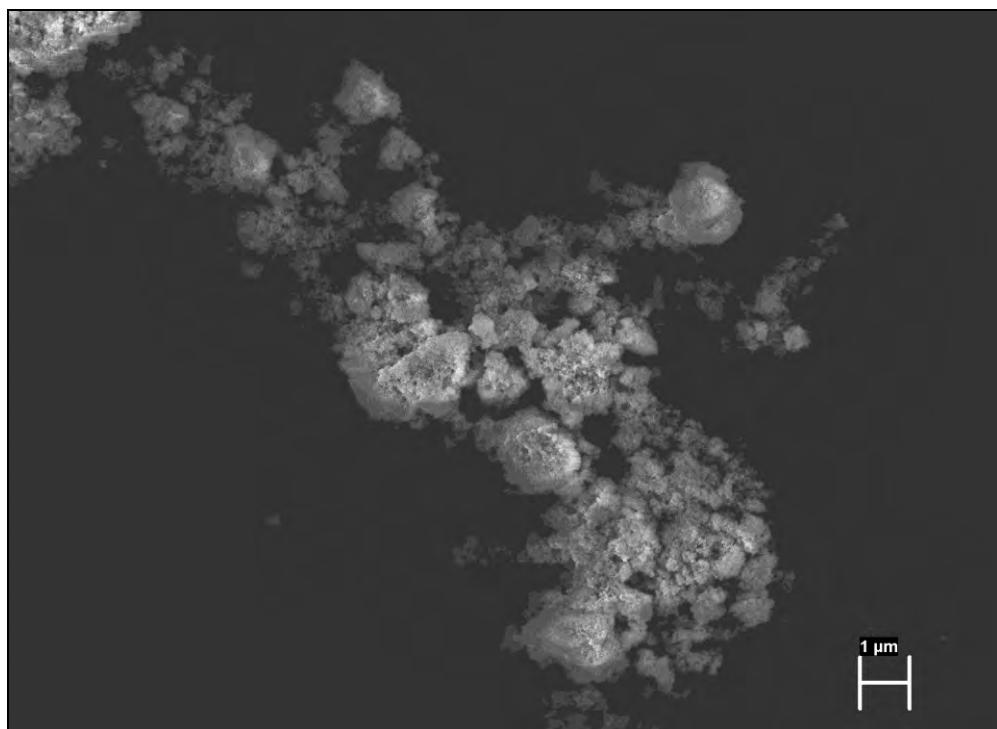
Figure 16.   SEM micrograph of the as-received ND powder showing typical agglomerate size.

Cursor Width = 10.92 µm
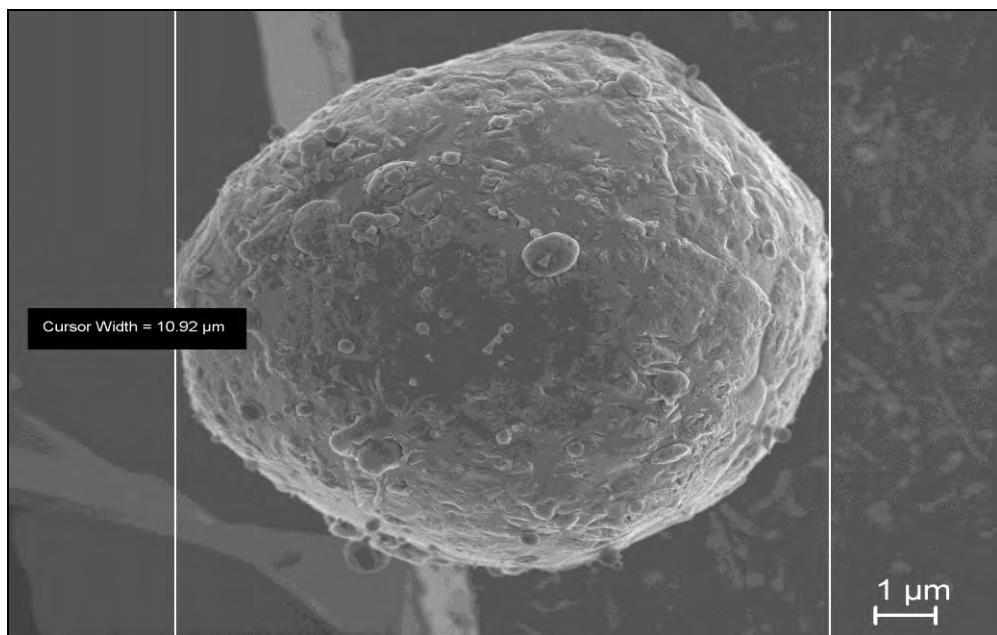
Figure 17.   SEM Micrograph of the as-received microaluminum powder particle illustrating the typical size.

2. Mechanically Alloyed Composite Powders

a. *Powder Morphology*

Average particle sizes for the milled composites tended to decrease in size as the milling time, ball-to-powder ratio and weight percentage of ND increased. Shown if Figure 18 is a series of SEM micrographs illustrating the powder morphologies of the 10:1, 5 wt% ND composite powders after being milled at the indicated times. As can be seen, with increasing milling time, the powder particles become more uniform and average particle size decreases. Furthermore, the rough, irregular surface of the milled powders is due to the repeated fracturing and cold welding that occurs during the milling process.
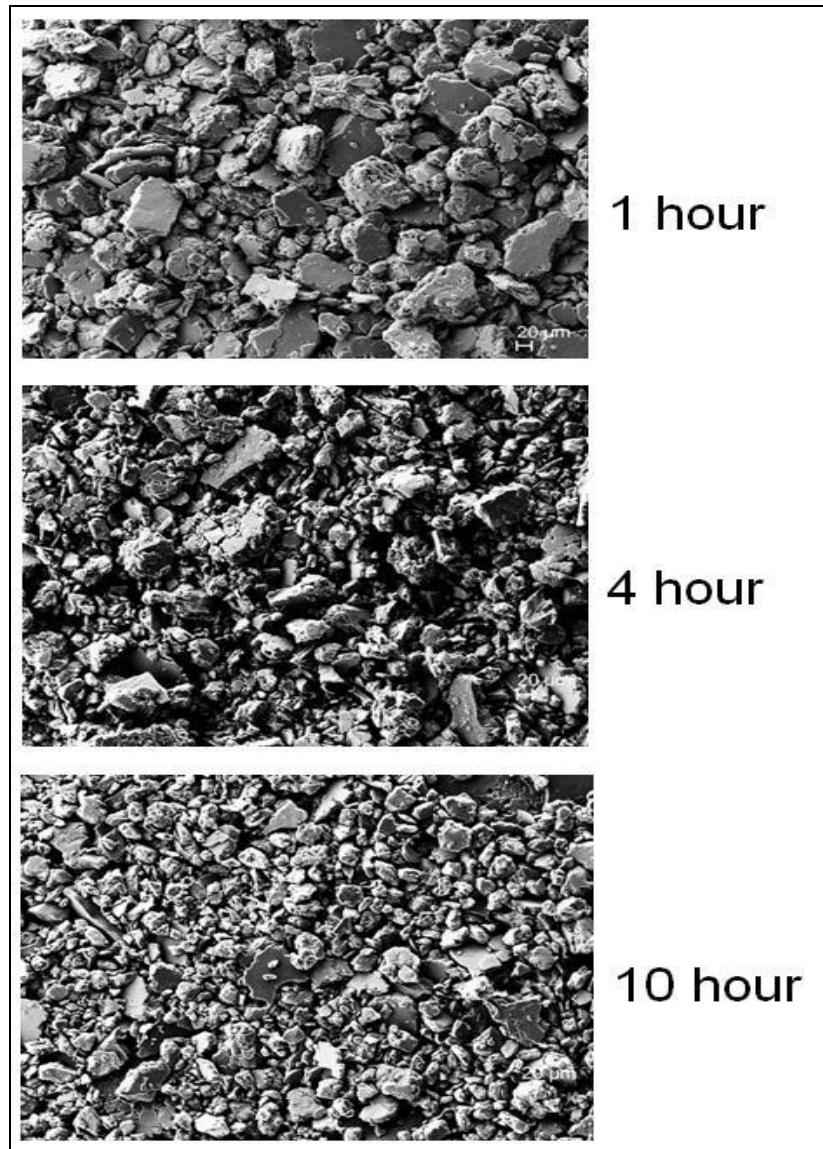
Figure 18.   Changes is particle size and uniformity as milling time increases for 5 wt% ND milled with a 10:1 ball-to-powder ratio. Other samples showed similar results.

Based on the results of the SEM micrographs of a number of samples, it was clear that the 10-hour samples had the most uniform appearance and had the smallest average particle sizes. Further characterization of the milled samples on the effect of ball-to-powder ratio and ND concentration was therefore conducted only on the 10-hour samples.

The data obtained from optical microscope images of 10-hour samples analyzed with Image-J showed that the average particle size varied only slightly when holding milling time and ND concentration constant and changing only the ball-to-powder ratio (Figures 19 and 20), however, the data also showed that the 30:1 ball-to-powder ratio produced the most uniform particle size, which can also be visually observed.
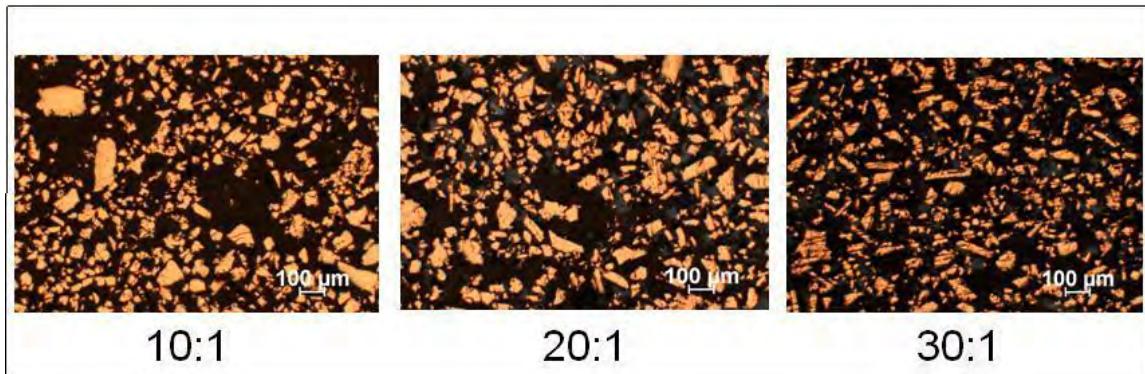

Figure 19.   Variation in particle size due to varying the ball-to-powder ratio for Al-5 wt% ND composite powder milled for 10 hours.
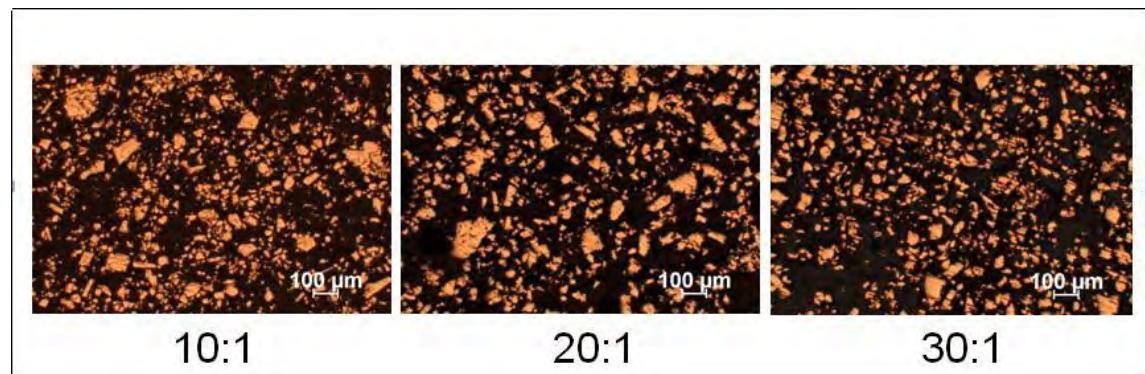

Figure 20.   Variation in particle size due to varying the ball to powder ratio for Al-10 wt% ND composite powder milled for 10 hours.

Additionally, the data showed that particle size also decreases with increasing ND concentration, which is likely due to the hardness of the composite increasing due to the homogenous dispersion of the ND, thereby minimizing cold welding, and increasing the likelihood of fracturing. As shown in Figure 21, powders with an average size of ~200 μm^2 were received after milling Al-10 wt%

ND composite powder for 10 hours, while the Al-5 wt% ND composite powder milled for the same time was ~360 μm^2. If we make the assumption that the particles are round, this correlates to an average diameter of ~16 μm for the Al-10 wt% ND composite powder and ~21.3 μm for the Al-5 wt% ND composite powder.
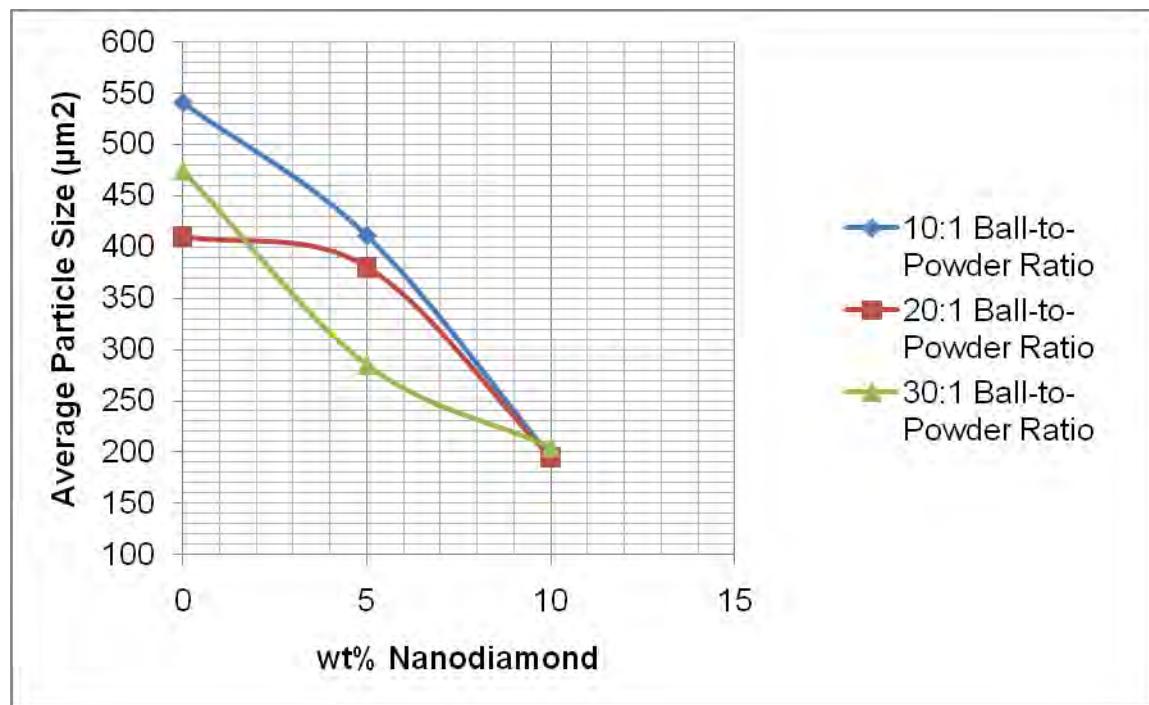

Figure 21. Average particle size (μm^2) vs wt% ND for 10 hour milled composite powders for the respective ball-to-powder ratios.

b.   *Chemical Composition*

To determine if there was a homogenous dispersion of NDs in the Al matrix, a series of EDS scans were run on three samples (1-, 4-, and 10-hour milling time at 10 wt% ND and 30:1 ball-to-powder ratio). Four particles from each sample were individually scanned as well as an overall scan of the entire sample. Shown in Figure 22 is a representative EDS spectrum from a large area scan on a ball-milled sample. As shown, there are only very minor carbon and oxygen signals, suggesting limited oxidation of the powders. Figure 23 shows the result of the EDS map made of a zoomed in view of single particle. All EDS

maps made of other particles and samples produced the same results. There are no obvious hot spots of carbon or oxygen noted which reinforces the notion that the ND agglomerates have broken down, but does not conclusively prove that there is a homogenous dispersion of ND in the Al matrix.
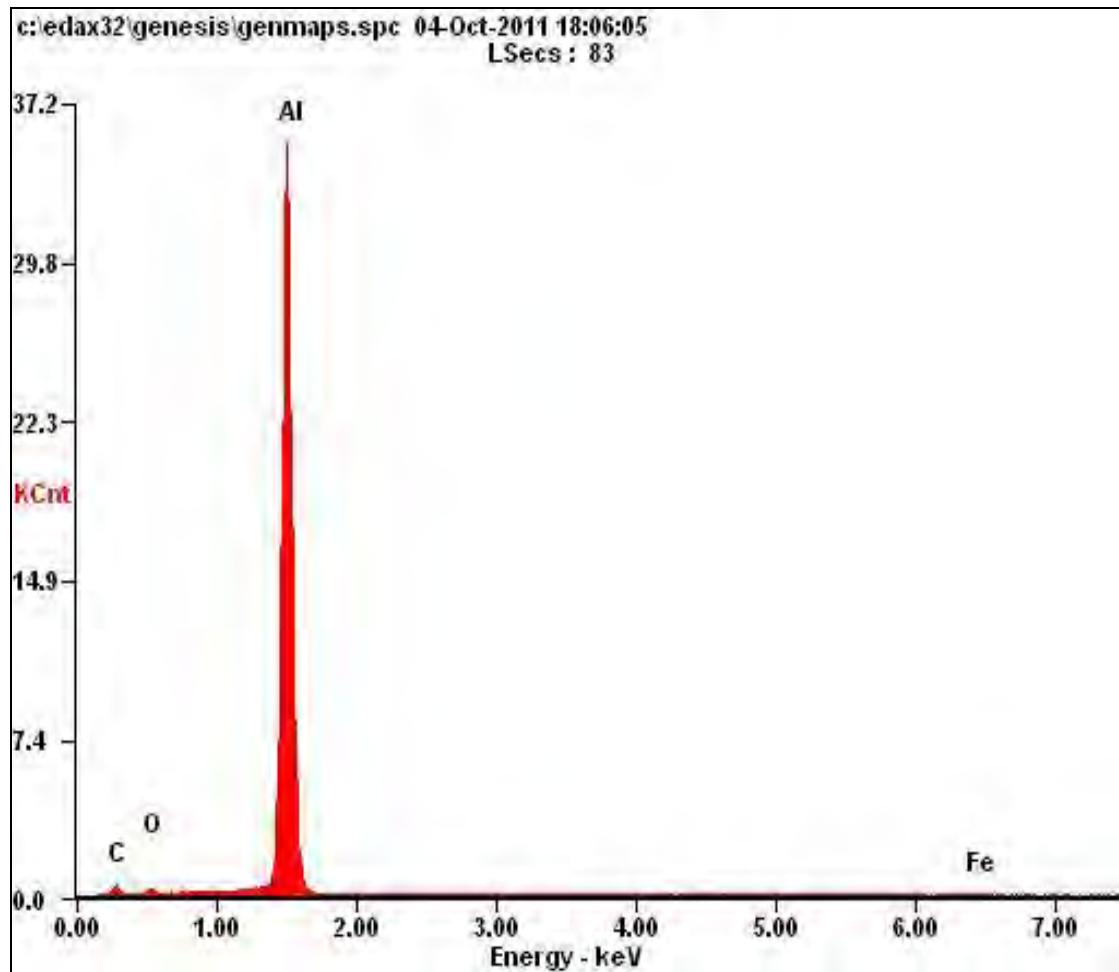

Figure 22.   EDS Scan of Al-5 wt% ND composite showing strong aluminum peak with negligible carbon and oxygen peaks.
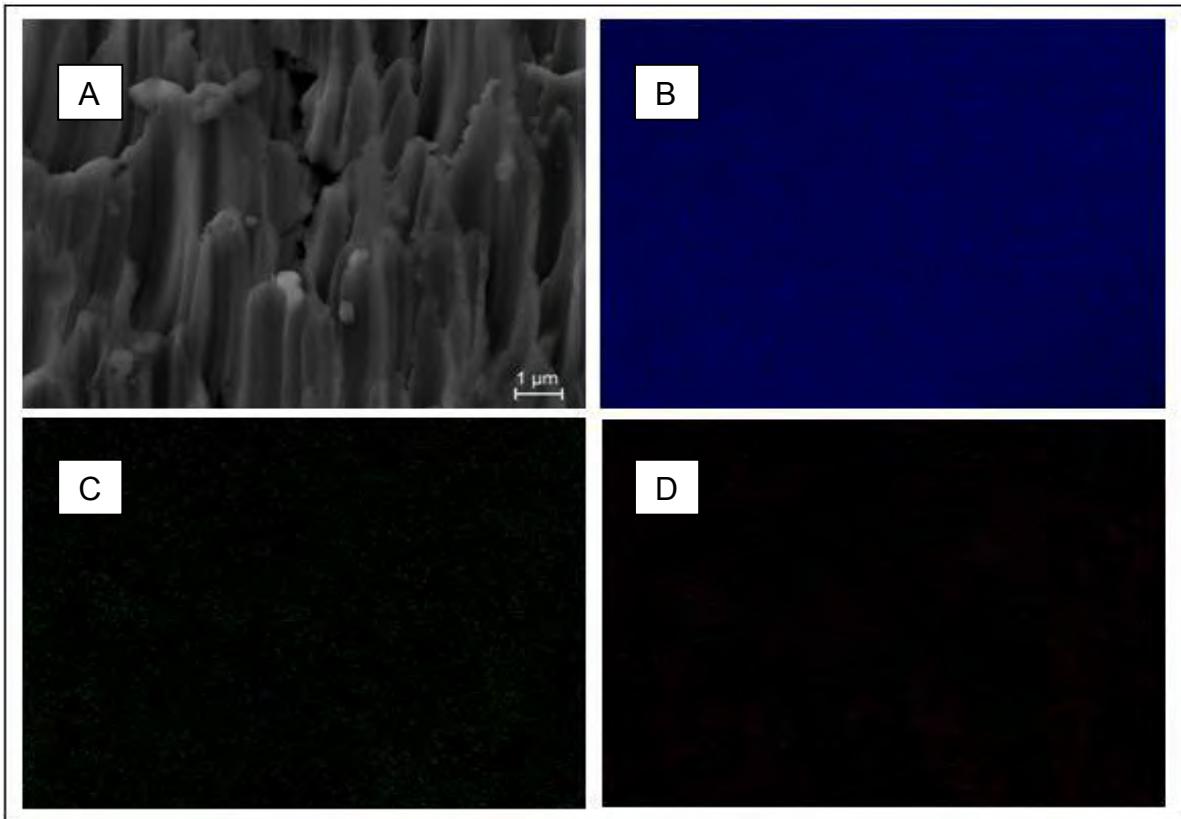
Figure 23. EDS map of a section of a typical milled composite particle (A) showing strong Al returns (B) with negligible returns on oxygen (C) and carbon (D).

C. GRAIN SIZE AND STRAIN ANALYSIS BY X-RAY DIFFRACTION

Figure 24 shows a typical XRD pattern of the composite powders. Every Al-ND composite sample showed only Al peaks. The weight fraction of ND was not high enough to be detectable, which further reinforces the assertion that the ND is homogenously dispersed in the aluminum matrix.
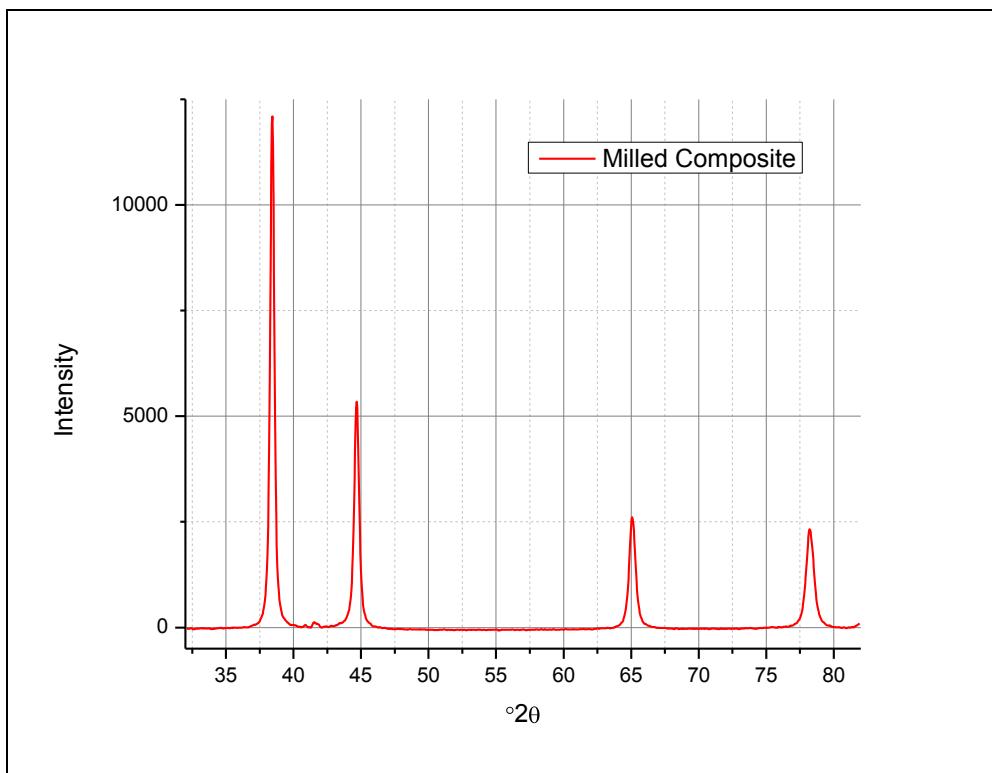
Figure 24.　Typical XRD diffraction pattern of milled nanocomposite.

The grain size and microstrain of all 27 samples was extracted from their respective powder diffraction profiles by using the W-H analysis discussed in Section II.　Figures 25 and 26 show the grain size and microstrain trends for the 5 wt% ND composite samples.　As can be seen, with the exception of the 20:1 sample, the grain size decreased until the four hour point, after which it began increasing.　This is likely due to a combination of increasing microstrain and work hardening of the material.
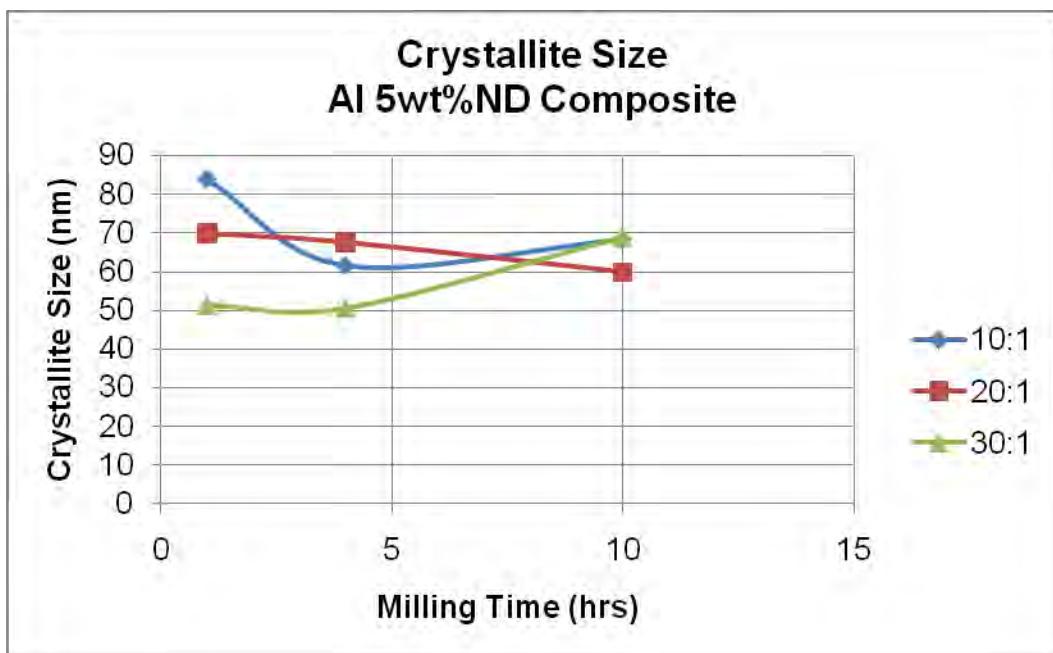
Figure 25.   Grain size vs milling time for each ball-to-powder ratio of the 5 wt% ND composite samples.
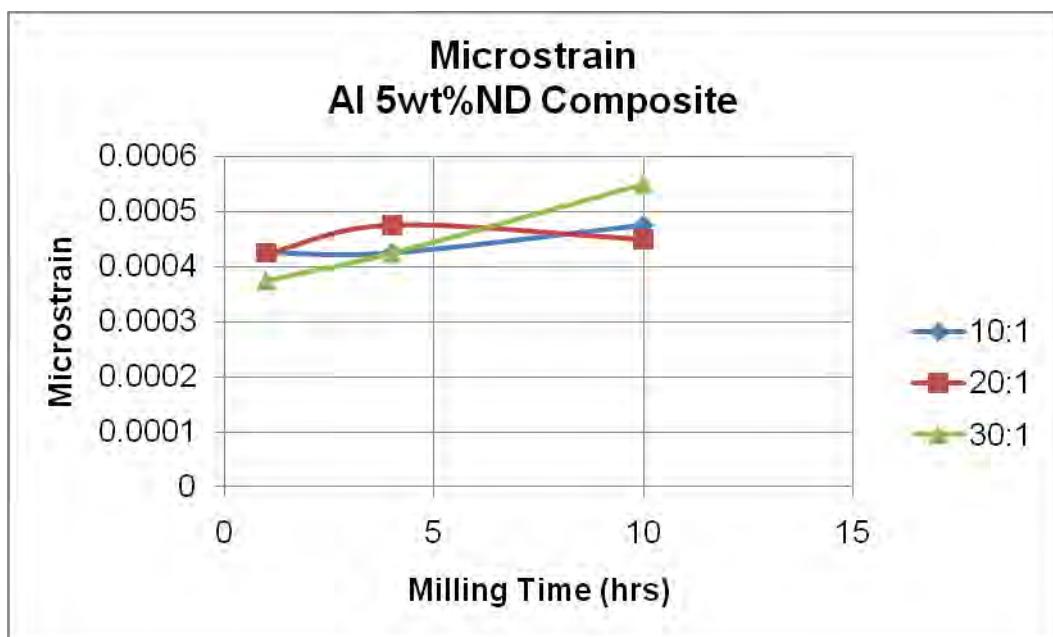

Figure 26.   Microstrain vs milling time for each ball-to-powder ratio of the 5 wt% ND composite samples.

Figures 27 and 28 show the grain size and microstrain trends for the 10 wt% ND composite samples. Unlike the 5 wt% ND samples, the 10 wt% ND samples show that the 30:1 ball-to-powder ratio produces the quickest decrease in particle size and is likely at its minimum at a half hour of milling time, whereas the 20:1 ball-to-powder ratio does not reach its smallest crystal size until the 4 hr point, and the 10:1 ball-to-powder ratio is still undergoing grain size reduction at the ten hour point. This trend is likely due to the larger concentration of ND increasing the strength of the composite powder.
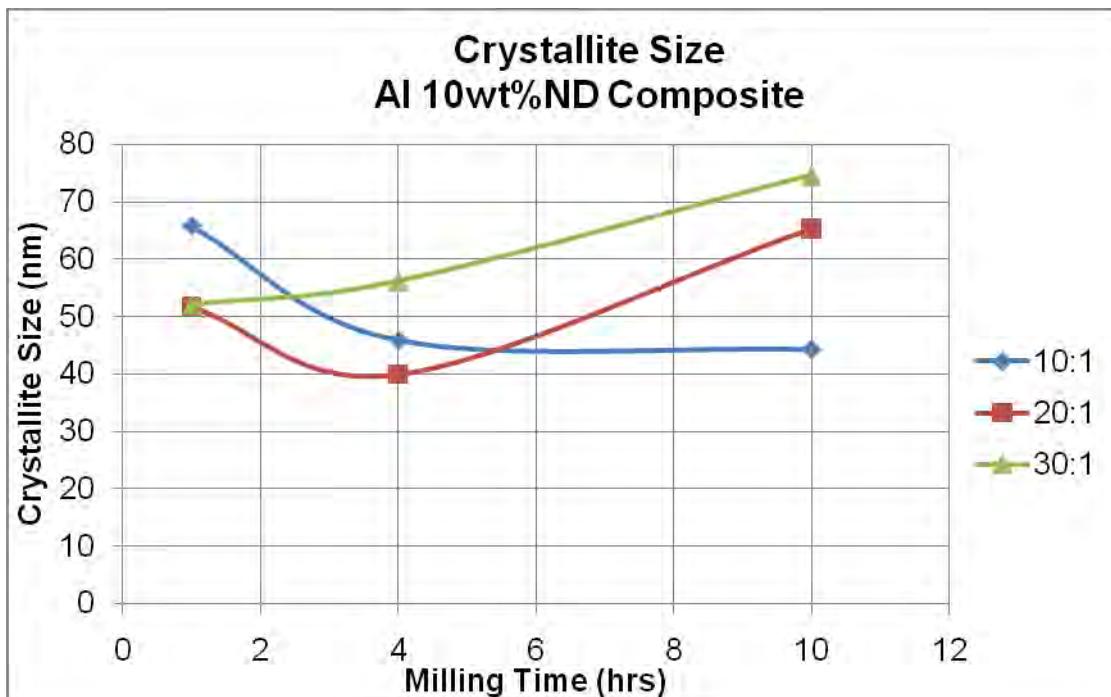

Figure 27.   Grain size vs milling time for each ball-to-powder ratio of the 10 wt% ND composite samples.
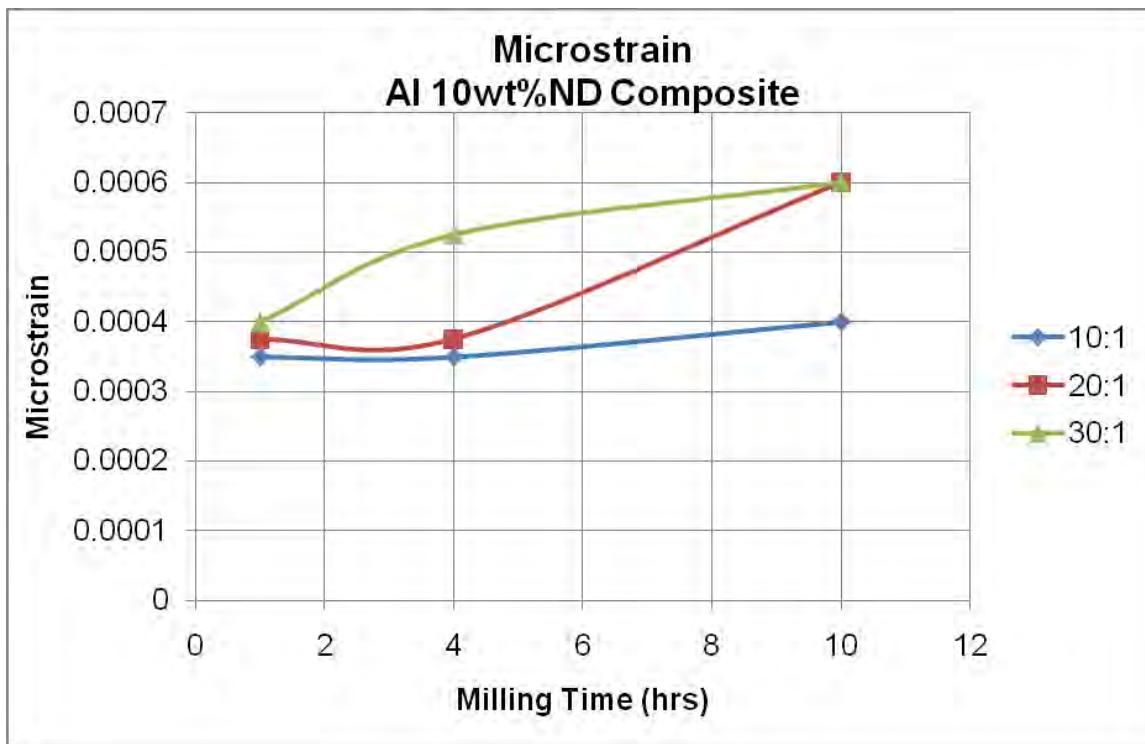
Figure 28. Microstrain vs milling time for each ball-to-powder ratio of the 5 wt% ND composite samples.

D. MECHANICAL PROPERTIES

Nanoindentation was used to try and determine some of the material properties of the Al-ND composite powders. Four samples were tested, with 11 particles from each sample being indented. The samples tested were the as-received Al powder and the 10-hour, 10:1 ball-to-powder ratio samples at 0, 5 and 10 wt% ND.

The elastic modulus results, shown in Figure 29 were substantially varied with no sample even approaching the 70 GPa elastic modulus of pure AL. These low modulus values are likely due to the effects of the epoxy mounting method and small particle size. Unlike the hardness measurement, as can be seen in the O-P equations discussed previously, the elastic modulus measurement is strongly influenced by the indentation surface area, so any load absorbed by the epoxy significantly alters the measured modulus. An investigation is currently in

progress to determine if the effect of the epoxy can be mitigated, but was not completed prior to the completion of this research.
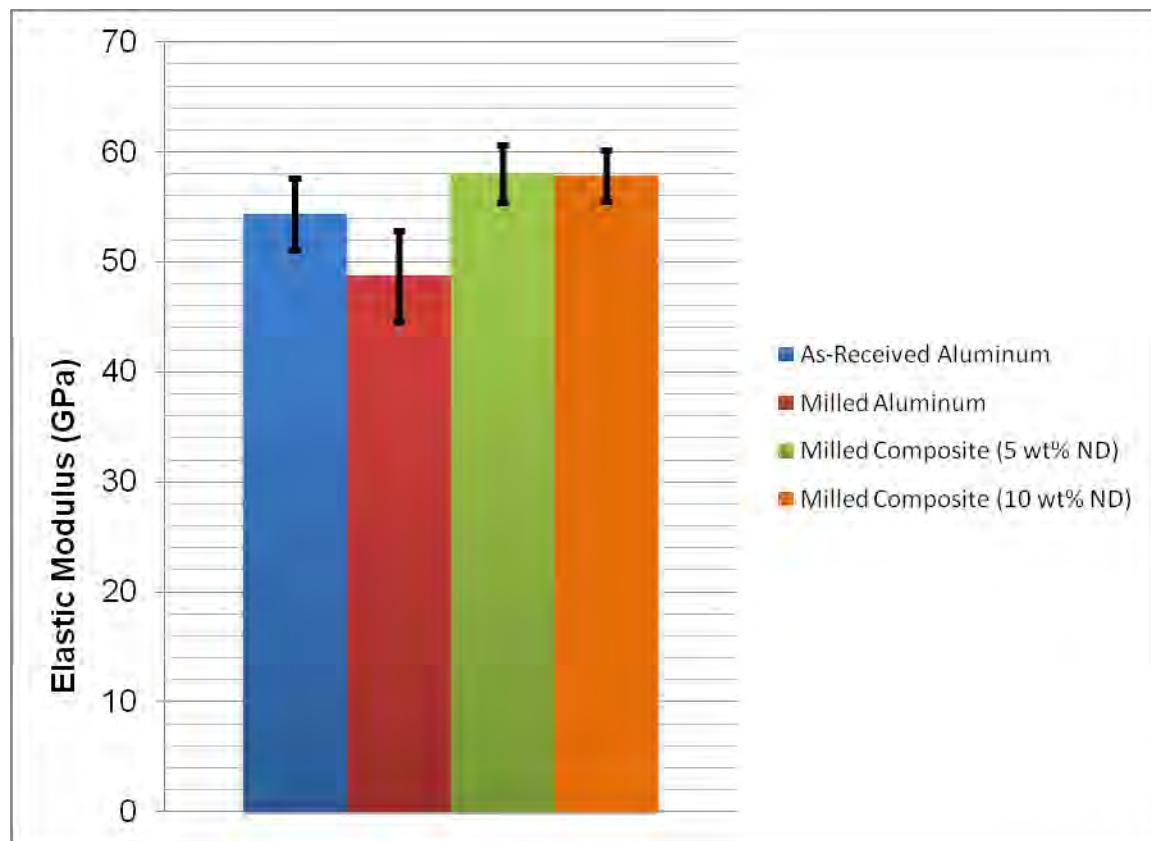
Figure 29.   Nanoindentation elastic modulus results of 10 hr milled, 10:1 ball-to-powder ratio samples showing inconclusive results.

As shown in Figure 30, the hardness measurements were very promising. The data showed that decreasing the grain size of the aluminum from ~150 nm to ~55 nm netted a 167% increase in hardness, which closely agreed with the Hall-Petch theory which predicted a 161% increase. Likewise, for the addition of ND, the Ashby-Orowan equation predicted 167% increase in hardness for the 5 wt% ND composite and 211% for the 10 wt% ND composite, The actual results showed a 134% increase for the 5 wt% ND composite and 163% increase for the 10 wt% composite.   Additionally, the hardness results also indicate there is a homogenous dispersion of the ND particulate.   Had the NDs agglomerated

without good dispersion, the hardness results of the 5 and 10 wt% ND samples should have been more in line with the milled Al sample.
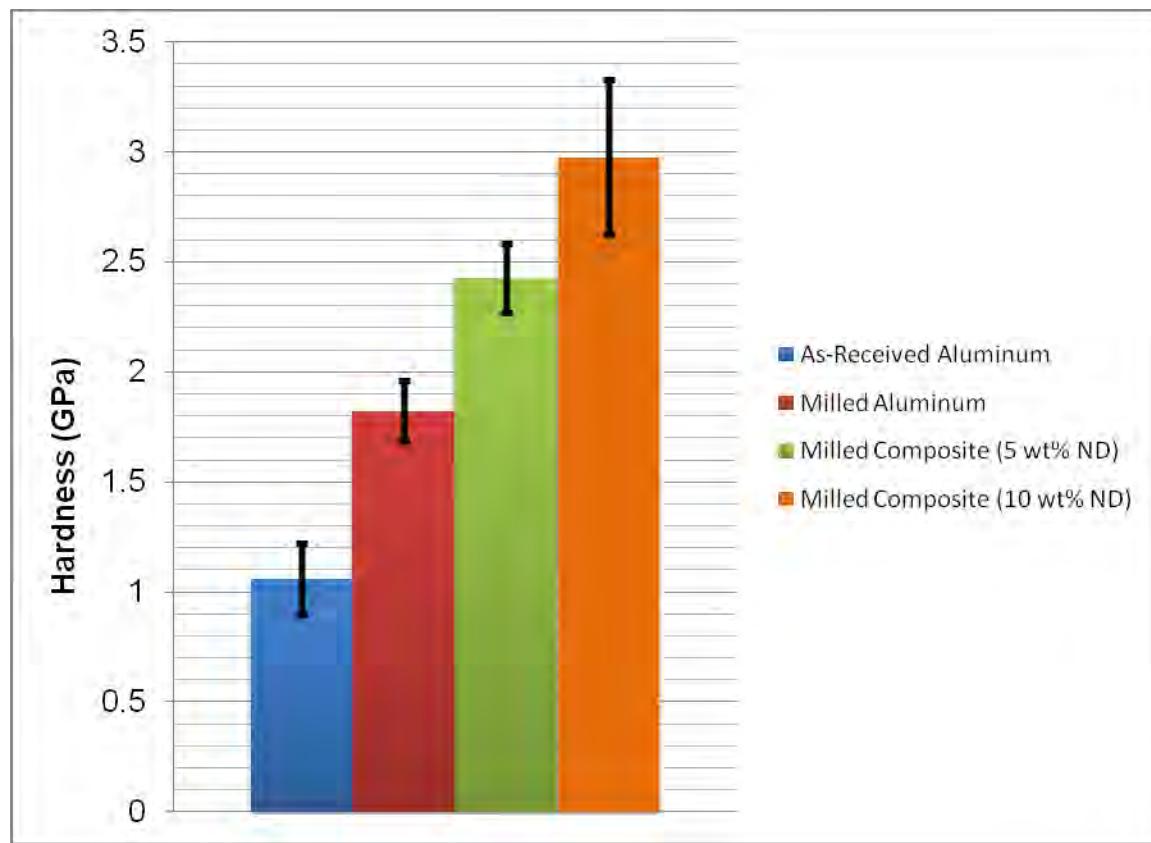

Figure 30.   Nanoindentation hardness results of 10 hr milled, 10:1 ball-to powder ratio samples showing upward trend and the concentration of ND is increased.

IV.   SUMMARY AND CONCLUSIONS

The results presented in this thesis mark the first Al-nanocarbon composite research efforts at the Naval Postgraduate School (NPS). Substantial progress was made in establishing the fabrication process and test methods of nanocarbon composite research, both of which lay the foundation for groundbreaking future nanocomposite research at NPS.

This research was successful in meeting the first thesis objective of determining if MA is a suitable technique for fabrication of an Al-ND composite powder for CS. As previous research indicated, and the results of this research show, MA via high energy ball milling is a robust method for producing a nanocrystalline material suitable for CS. The sustained mechanical fracturing and deformation significantly reduced the grain size and increased the material's stored energy, thereby leading to large increases in strength. Additionally, there were no phase changes noted in any of the ball milled nanodiamond samples which indicates that the milling process is not damaging their nanostructure. Strengthening is realized by grain size refinement and dispersion strengthening, in the case of the Al-ND composite.

The second objective, determining how milling parameters affect the structure and properties of the composite powders, was also successful. The research showed that for the experiments we performed, a 10-hour milling time and 30:1 ball to powder ratio yielded the smallest and most consistent particle sizes with good dispersion of the ND particulates. Although the 4-hour milled samples showed the most grain size reduction overall, the 10-hour samples were still sufficiently small and the more consistent particle sizes would be the best for CS processing. Additionally, all characterization methods used, especially EDS and nanoindentation, indicated that there was a homogenous dispersion of the ND particulate in the Al matrix. Additionally, as shown by nanoindentation, high energy ball milling increased the hardness of the as-received Al by approximately

167%. When 5 wt% and 10 wt% ND was added to form an Al-ND composite, the hardness increased 134% and 163% respectively. Unfortunately, the results of the elastic modulus measurements were inconclusive, likely due to the effects of the epoxy mounting method.

In this study, EDS was the only method used to quantify the homogenous dispersion of the ND particulate, and unfortunately, the data was not conclusive. Additionally, XRD was the only method used to quantify grain size. While both methods gave useful results, when characterizing any material, especially nanocrystalline materials, more than one method should be used. Verification of the grain size and homogenous dispersion of ND particulate could both be verified through the use of transmission electron microscopy (TEM). Additionally, TEM could also give the grain size distribution and shape. TEM of the nanocomposite studied in the research was not carried out due to time constraints.

CS is hoped to be a good method to consolidate the composite powder. Further mechanical testing cannot realistically occur until the powder is consolidated into a solid form

LIST OF REFERENCES

[1]   J. Montgomery, et al, "Low-cost titanium armors for combat vehicles," *JOM*, vol. 49, no. 5, pp. 45–47, 1997.

[2]   M. Myers and K. Chawla, "Grain Boundaries in Plastic Deformation (Grain-Size Strengthening)," in *Mechanical Behavior of Materials, 2*nd ed., Cambridge, UK, Cambridge Univ. Press, 2009, ch. 5, sec. 4, pp. 345–348.

[3]   M. Huller, G. Chernik et al, "Mechanical alloying in planetarty mills of high accelerations," *Rev. Adv. Mater. Sci.*, vol. 18, pp. 366–374, 2008.

[4]   B. Q. Han, et al, "Tension and compression behaviors of bulk ultrafine-grained Al-7.5wt% Mg alloy," *Philosophical Magazine Letters*, vol. 83, no. 2, pp. 89–96, 2003.

[5]   L. Kollo, et al, "Nano-silicon carbide reinforced aluminium produced by high-energy milling and hot consolidation," *Materials Science and Engineering A*, vol. 528, pp. 6606–6615, 2011.

[6]   C. C. Koch, "Synthesis of Nanostructured Materials by Mechanical Milling: Problems and Opportunities," *Nanostructured Materials*, vol. 9, pp. 13–22, 1997.

[7]   G. S. Upadhyaya, "Hot Consolidation," in *Powder Metallurgy Technology*, Cambridge, UK: Cambridge International Sci. Pub., 1996, ch 7, sec. 1, pp. 96–99.

[8]   C. C. Koch, "Nanocrystalline powder consolidation methods," in *Nanostructured Materials: Processing, Properties and Potential Applications*, Norwich, NY: William Andrew Pub., 2002, ch. 4, sec. 3, pp. 155–156.

[9]   *Handbook of Thermal Spray Technology*, ASM International, Materials Park, OH, 2004, pp. 77–84.

[10]   T. D. Shen and C. C. Koch, "Formation, solid solution hardening and softening of nanocrystalline solid solutions prepared by mechanical attrition," *Acta Materialia*, vol. 44, no. 2, pp. 753–761, 1996.

[11]   Y. Zhang, et al, "Cold-spray processing of high density nanocrystalline aluminum alloy 2009 coating using a mixture of as-atomized and as-cryomilled powders," *Journal of Thermal Spray Technology*, vol. 20, no. 5, pp. 1125–1131, 2011

[12]   C. Suryanarayana, "Mechanical alloying and milling," *Progress in Materials Science*, vol. 46, pp. 1–184, 2001.

[13]   D. Witkin, et al "Al-Mg alloy engineered with bimodal grain size for high strength and increased ductility," *Scripta Materialia*, vol. 49, pp. 297–302, 2003.

[14]   H. J. Fecht, "Nanostructure formation by mechanical attrition," *Nanostructured Materials*, vol. 9, pp. 33–42, 1995.

[15]   C. DeCastro and B. Mitchell, "Nanoparticles from Mechanical Attrition," in *Synthesis, Functionalization and Surface Treatment of Nanoparticles*, M. Baraton, Ed. Valencia, CA: American Scientific Publishers, 2002, pp 1–15.

[16]   F. Zhou, et al, "Formation of nanostructure in Al produced by a low-energy ball milling at cryogenic temperature," *Materials Science and Engineering A*, vols. 375-377, pp. 917–921, 2004.

[17]   A. J. Maisano, "Cryomilling of aluminum-based and magnesium-based metal powders," M. S. thesis, Dept. Matl. Science, Virginia Polytechnic Inst., Blacksburg, VA, 2006.

[18]   C. Patino-Carachure, et al, "Electron Microscopy Characterization of Humidity Ball-Milling AlCuFe Intermetallic Powders," *Mater. Res. Soc. Symp. Proc.*, vol 1242, 2010.

[19]   S. Filho, et al, "Synthesis of diamond reinforced Al-Mg nanocrystalline composite powder using ball milling," *Materials Science Forums*, vols. 416-418, pp. 213–218, 2003.

[20]   D. Oleszak and P. Shingu, "Nanocrystalline metals prepared by low energy ball milling," *Journal of Applied Physics*, vol. 79, no. 6, pp. 2975–2980, 1996.

[21]   L. Ajdelsztajn, et al, "Cold spray deposition of nanocrystalline aluminum alloys," *Metallurgical and Materials Transactions*, vol. 36A, no. 3, pp. 657–666, 2005.

[22]   B. D. Cullity, *Elements of X-Ray Diffraction*, Reading, MA: Addison-Wesley Pub. Co. Inc., 1978.

[23]   B. L. Gabriel, *SEM: A User's Manual for Materials Science.* Metals Park, OH: American Society For Metals, 1985.

[24]   M. Myers and K. Chawla, "Nanoindentation," in *Mechanical Behavior of Materials,* 2nd ed., Cambridge, UK, Cambridge Univ. Press, 2009, ch. 3, sec. 8, pp. 225–229.

[25]   W. C. Oliver and G. M. Pharr, "An improved technique for determining hardness and elastic modulus using load and displacement sensing indentation experiments," *Journal of Materials Research*, vol. 7, no. 6, pp. 1564–1583, 1992.

THIS PAGE INTENTIONALLY LEFT BLANK

INITIAL DISTRIBUTION LIST

1. Defense Technical Information Center
    Ft. Belvoir, Virginia

2. Dudley Knox Library
    Naval Postgraduate School
    Monterey, California